BEAM DIAGNOSTICS

Ulrich Raich

Beam Instrumentation (BI) Group

Beams (BE) Department CERN, Geneva Switzerland

Abstract

The instrumentation measuring beam parameters constitutes an important part in any particle accelerator. These lectures aim at giving an overview of detection and measurement techniques without going too much into implementation details. A number of instruments used to measure basic beam parameters like intensity, beam position or beam profile is described before explaining the measurement of more elaborate accelerator parameters like tune and transverse or longitudinal emittance.

1. INTRODUCTION

An accelerator can never be better than the instruments which measure its performance! Measurement instruments play a vital role in the operation of an accelerator. They are particularly important when new machines are commissioned (a moment when new instruments are also tried for the first time!) or at startup after a long shutdown. However also during routine machine operation it is the beam measurements that tell the operator if the machine is performing correctly or not and it is the instruments that will help him to find potential faults in accelerator components.

Beam diagnostics covers a large field of activity: Some knowledge of machine physics is needed in order to understand the machine parameters to be measured and the physical effects that govern their behavior. The physics of beam interaction with the measurement sensors must be understood in order to build the sensor itself. Highly sensitive analogue electronics are needed in order to amplify usually very small signals which in addition are often very fast. Digitization and digital treatment of the signals must be performed and finally a result in form of a complex beam parameter value, like the tune, the transverse - or longitudinal emittance, the beam orbit etc. must be extracted and displayed, requiring experience in software technologies.

Instrument	**Physical Effect**	**Measured Quantity**	**Effect on the beam**
Faraday Cup	Charge Collection	Intensity	Destructive
Current Transformer	Magnetic Field	Intensity	Non destructive
Wall Current Monitor	Image Current	Intensity, longitudinal density distribution	Non destructive
Pick-up, beam position monitor (BPM)	Electric/magnetic Field	Position, trajectory, orbit	Non destructive
Secondary Emission Monitor	Secondary electron emission	Transverse profile, intensity, emittance	Disturbing, at low energy: destructive
Wire Scanner	Secondary emission, creation of secondary particles	Transverse profile, emittance	Slightly disturbing
Scintillator screen	Atomic excitation with light emission	Transverse profile, position	Destructive
Residual Gas Monitor	Ionization	Transverse profile	Non destructive

Table 1-1: Instruments, measured quantities and physical effects used

Most sensors are based on one of the following physical processes:

- Interaction with electric or magnetic fields of the beam particles
    - Coupling to the magnetic or electric field
    - Synchrotron radiation
    - Transition radiation

- Coulomb interaction between the incident beam particle and electrons in the atomic shell of intercepting matter
- Atomic excitation with consecutive light emission

Table 1-1 lists some of the instruments used in beam diagnostics, the physical effect made use of and the beam parameter measured.

A typical instrument consists of

- the sensor (see Figure 1-1)
- its front end electronics, usually a pre-amplifier and shaper installed in the machine tunnel
- cabling between the tunnel and the equipment room
- signal treatment electronics and analogue to digital conversion in the front-end computer crate
  this may also include some digital input/output e.g. for status information or digital control (end switches, electronics on/off, vacuum status, amplifier gain control …)
- front-end software to read out the digital data and perform digital signal treatment
- application software running on console computers in the main control room

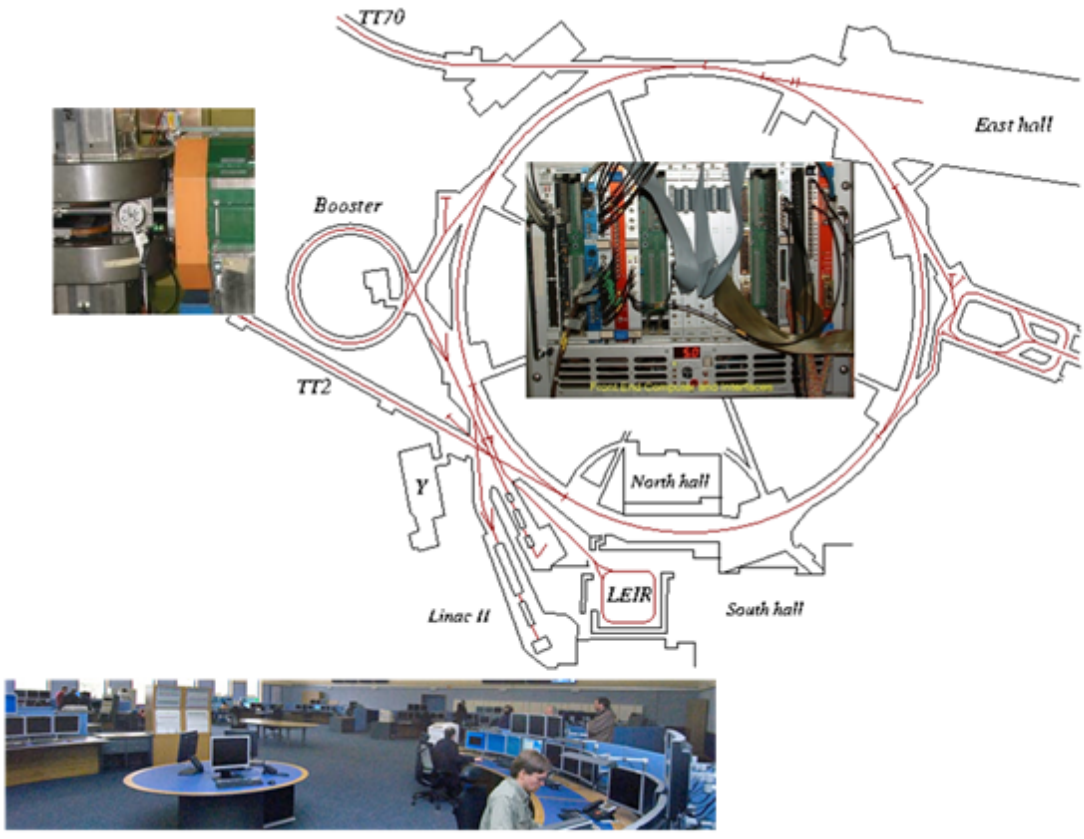

Figure 1-1: A typical instrument:

2. INTENSITY MEASUREMENTS

2.1 Faraday Cups

At very low energies and low intensities the Faraday Cup is an often used device for intensity measurements. It acts as a beam stopper and is therefore fully destructive. An insulated metallic cup is connected to either an integrating amplifier measuring the number of incoming charges or a current sensitive amplifier in which case the beam current is measured. A typical setup is shown in Figure 2-1 and Figure 2-2.

Very low intensities down to a few pA can be measured, even for a DC beam, with low noise current to voltage amplifiers.

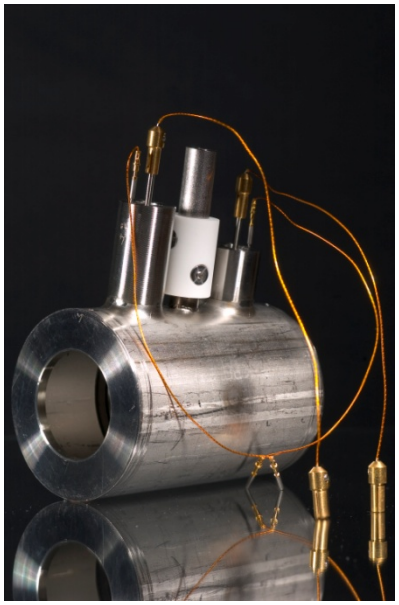

Figure 2-1: Photo of Faraday Cup

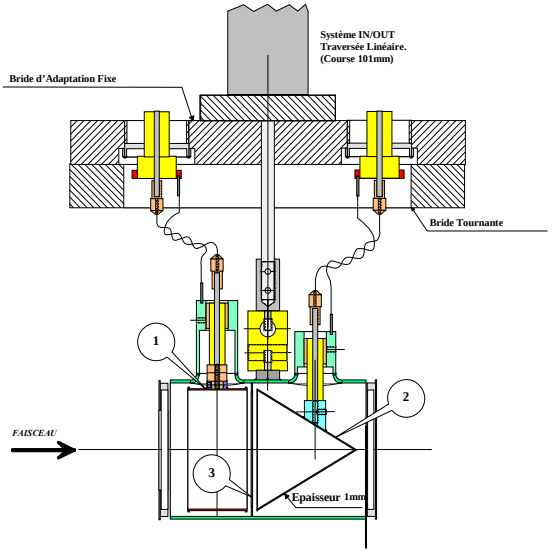

Figure 2-2: Drawing of the Faraday Cup

When a particle hits the cup's electrode surface, secondary electrons are emitted. Typical yields for incident protons of 50KeV, taking into account the cup's opening angle of 60^0, are 6-7 electrons per incoming proton. The energy of these secondary electrons is very low (below 10 eV) and their flux is proportional to cos θ, where θ is the angle of the emitted electron with respect to the electrode surface. Because of their low energy the electrons can be re-captured into the cup by applying HV to a repeller electrode. A simulation of the electro-static field within the cup when applying a -100V repelling voltage is shown in Figure 2-3, the effect on the measured current when increasing the voltage from 0 up to -100V is displayed in Figure 2-4.

The Faraday Cup described above has a stainless steel electrode of 1 mm thickness. Protons with energy higher than 24 MeV will traverse the electrode and their charge will therefore not be captured, leading to wrong measurement results.

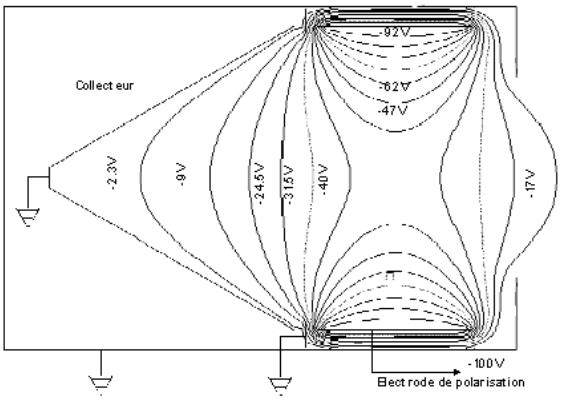

Figure 2-3: Electrical field simulation in the Faraday Cup with the repeller voltage on

Increasing the beam energy and/or intensity will increase the thermal load that must be absorbed by the cup. The choice of material (high thermal conductivity) will become important and means of cooling, e.g. water cooling, may need to be introduced.

A typical application for Faraday Cups is the measurement of charge-state-distributions coming from a heavy ion source. The source produces a spectrum of some 20 different ionization states from which a single one will be selected for further acceleration.

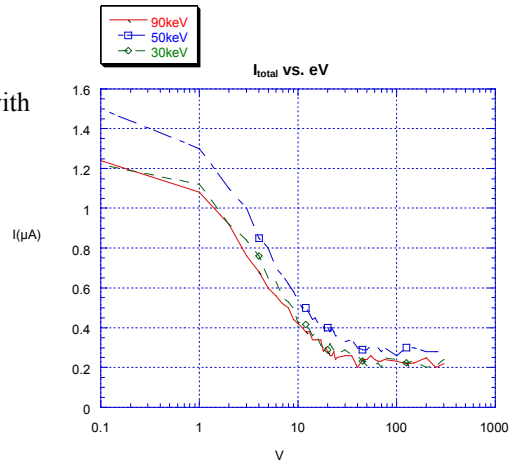

Figure 2-4: Electrode current versus of repeller voltage

The measurement uses a spectrometer magnet deflecting each of the ions with different charge state in a different way and a slit, selecting a fine slice in the spectrum. The spectrometer magnet is ramped and the current passing though the slit is recorded with a Faraday Cup. Figure 2-5 shows a typical result for lead ions. (The negative values probably come from the beam, striking the repeller electrode which produces secondary electrons seen by the Faraday Cup).

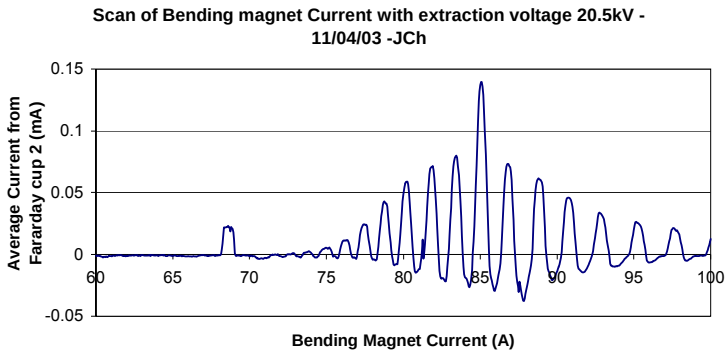

Figure 2-5: Charge State spectrum from a lead ion source measured with a Faraday Cup

2.2 **Current Transformers**

As we know from school physics moving charges create a magnetic field which is proportional to the current. Since a particle beam is nothing else than a collection of moving charges, it forms a current which can be described by $I_{beam} = \frac{qeN}{t} = \frac{qeN\beta c}{l}$ where q is the charge state, N the number of particles, l unit of length and $\beta = \frac{v}{c}$ the particle speed.

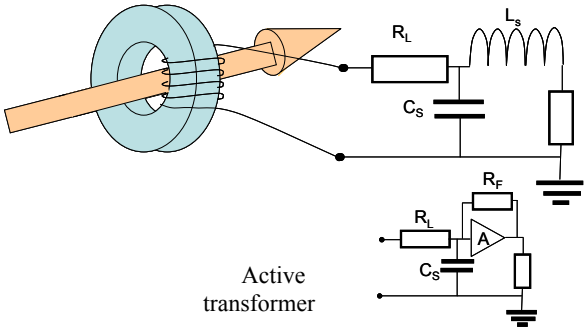

Figure 2-6: Principle of a DC current transformer

The magnetic field associated with this beam can be captured using a transformer which will deliver a voltage $U = L\frac{dI_{beam}}{dt}$ in the ideal case and with infinite output impedance (see Figure 2-7a). If however we load the transformer with a finite resistance and we take into account secondary inductance and capacitance then we get a pulse shape of the form:

$$u(t) = I_{beam}(t)\frac{R}{N}e^{-\frac{t}{\tau_{droop}}}.$$

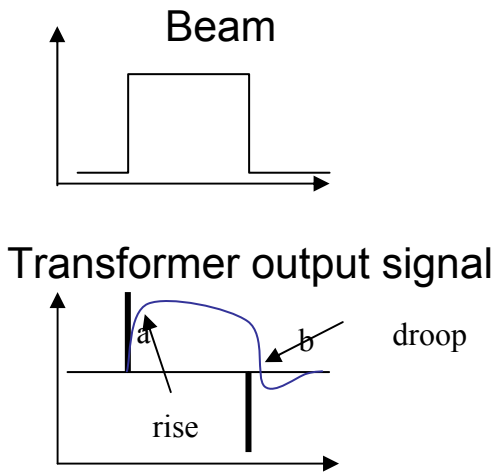

Figure 2-7: The ideal output signal from an AC current transformer
a) infinite output impedance
b) finite output impedance with stray capacitance and inductance

The rise-time of the output signal is determined by cable inductance and stray capacitance: $\tau_{rise} = \sqrt{L_s C_s}$ and the droop time constant by the cable inductance and the output impedance: $\tau_{droop} = \frac{L}{R + R_L}$. By using an active transformer in which the output resistor is replaced by an operational amplifier with gain A and a feedback resistor R_f the droop time can be extended until up to a second.

$$\tau_{droop} = \frac{L}{\frac{R_f}{A} + R_L} \approx \frac{L}{R_L}.$$

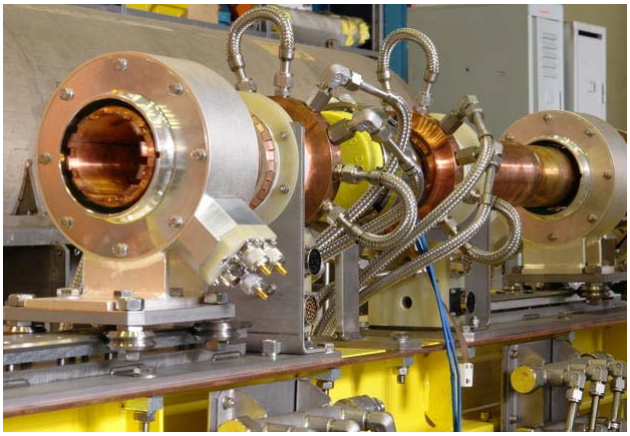

Figure 2-8: Photo of LHC AC current transformer

Figure 2-9: Constituents of the LHC AC current transformer

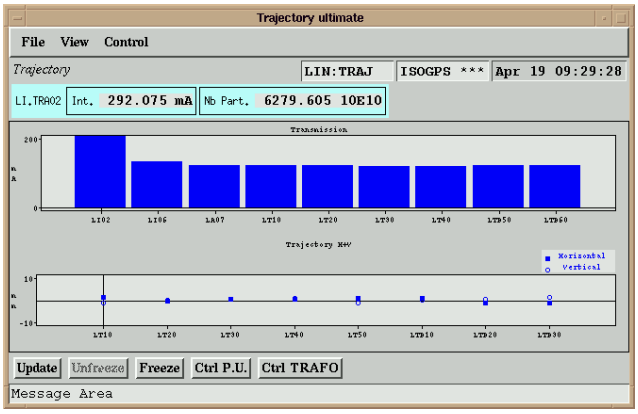

Figure 2-10: Beam losses seen by current transformer

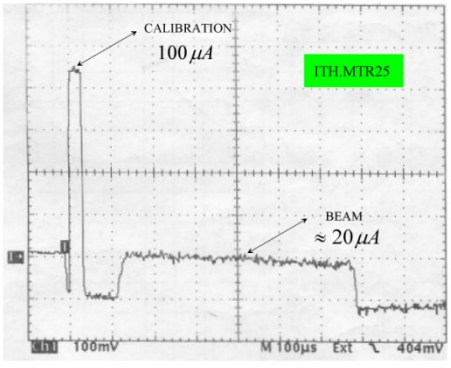

Figure 2-11: Calibration and beam pulse on an AC current transformer

In low energy machines the beam needs to be re-focused in a tight mesh of focusing magnets leaving little space. This implies that the instruments may be situated close to high powered pulsing equipment which will cause electro-magnetic interference. The transformer is therefore enclosed in shielding layers consisting of soft iron and μ-metal layers.

At low energy we often have beam pulses of several hundred μs length which can easily be digitized with a fast analogue to digital converter. The converted signal can then be treated digitally; baseline shifts due to surrounding elements can be determined and corrected for.

The transformer must be calibrated, which is usually done with a high precision current source. The current signal is injected into the transformer through a separate calibration winding. This may be done only once in a dedicated calibration procedure where the results are stored in tables and re-used by the read-out program. It can however also be done for each beam pulse by injecting the signal shortly before or after the arrival of the beam pulse and reading it with the measurement data (Figure 2-11).

Figure 2-10 shows a typical transformer measurement: The beam intensity (bar graph) is observed along a transport line and losses between 2 transformers can be easily spotted.

2.3 **DC current transformers**

In order to extend the transformer's bandwidth down to DC, needed e.g. for storage rings, in which the beam may stay for hours, the principle of the zero flux magnometer is applied. Is uses a magnetic modulator exploiting the non-linear magnetization curve of ferro-magnetic material. Two cores are fed in opposite phase with a modulation current driving the cores into saturation. The signals from secondary windings connected in series will produce a zero sum signal. Since the magnetization curve will be perfectly symmetric, only odd harmonics of the modulation frequency will be present in the modulation spectrum. It is clear that the pair of coils must be carefully matched such that the induced signal after subtraction is minimized.

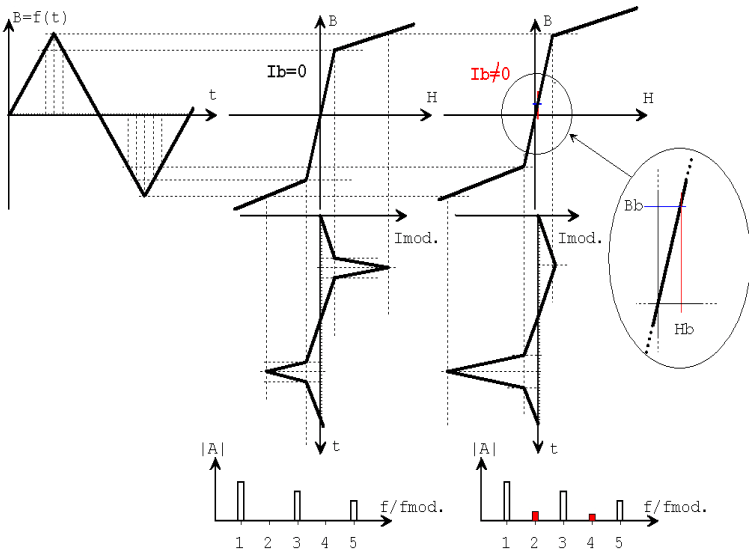

Figure 2-12: Modulation of a DCCT

left: without beam, right: with beam

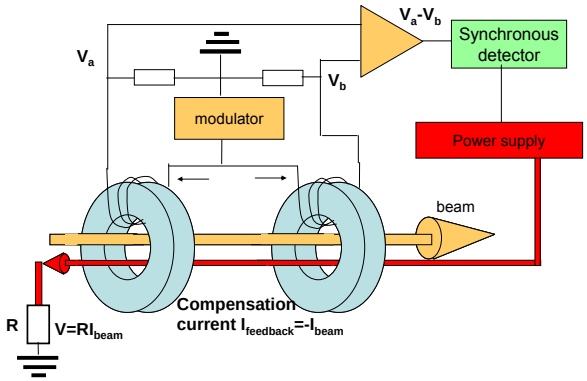

Figure 2-13: Zero flux magnetometer

A DC current passing through the coils introduces a bias in the excitation, the sum signal becomes non zero and even harmonics, in particular the second harmonic, will appear in the spectrum.

A synchronous detector extracts the information about the signal amplitude and phase of the component at the second harmonic of the modulation frequency. This signal is used to create a feedback current cancelling the flux induced by the beam. The feedback current is finally measured.

When measuring beam intensity in low energy synchrotrons, it is actually not the DC current but the number of particles or number of charges which is the parameter of interest. Since the revolution frequency changes due to the increasing speed of the particles, the current will also increase. One can extract the number of charges by calculating the particle speed from the measured magnetic field of the synchrotron's bending magnets and applying β-normalization.

Figure 2-14 shows the LHC DC current transformer. The outer 2 cores are used for the zero flux magnometer while the inner core is in fact an AC current transformer extending the bandwith to higher frequencies.

Figure 2-14: LHC DC current transformer

3. PROFILE AND EMITTANCE MEASUREMENTS

3.1 Interaction of a particle beam with matter

Most of the profile measurement devices rely on an intercepting sensor to generate a signal containing the information of beam density at a certain position or angle. The signal may be the emission of light or it may be a current created through the ionization of a gas or through secondary emission of electrons from the material's surface. In order to estimate the signal power, we must look into the mechanism of energy transfer from the accelerated particle to the intercepting matter.

All the effects result from Coulomb interaction of the incoming beam particles with the sensor matter.

When a beam particle at high speed passes near an atomic shell electron of the intercepting material, the force F_s along the particle's path cancels, while the transverse force does not. This means that ejected electrons will be observed at right angles with respect to the beam particles' movement. Head-on collisions (with very small impact parameter b, where electrons have high energies (delta electrons)) are very rare and the electron energy is generally below 20 eV.

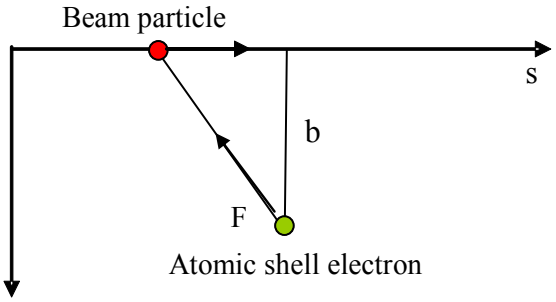

Figure 3-1: Beam particle interacting with atomic shell

The energy loss of an ionizing particle in matter is described by the Bethe-Bloch formula:

$$-\frac{dE}{dx} = 4\pi\, N_A r_e^2 m_e c^2 \frac{Z_T}{A_T} \rho \frac{Z_p^2}{\beta^2} \left[\ln \frac{2 m_e c^2 \gamma^2 \beta^2}{I} - \beta^2\right]$$

with the following constants:

- N_A: Avogadro's number
- m_e and r_e: electron rest mass and classical electron radius
- c: speed of light

the following target material properties:

- ρ: material density
- A_T and Z_T: the atomic mass and nuclear charge

and the particle properties:

- Z_p: particle charge
- β: the particles velocity and $\gamma = \frac{1}{\sqrt{1-\beta^2}}$

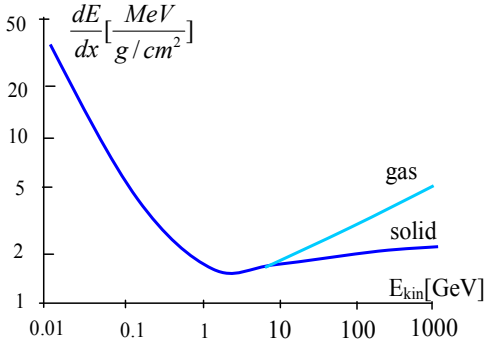

Figure 3-2: The Bethe Bloch Formula

Two facts are interesting to note: The quadratic dependence on the particle charge, meaning that the energy deposition of high charge state heavy ions is much higher than e.g. for singly charged protons and the fact that low energy particles deposit much more energy in

the target material than higher energy ones. At ~1GeV a projectile particle is called minimum ionizing because its energy transfer is at a minimum.

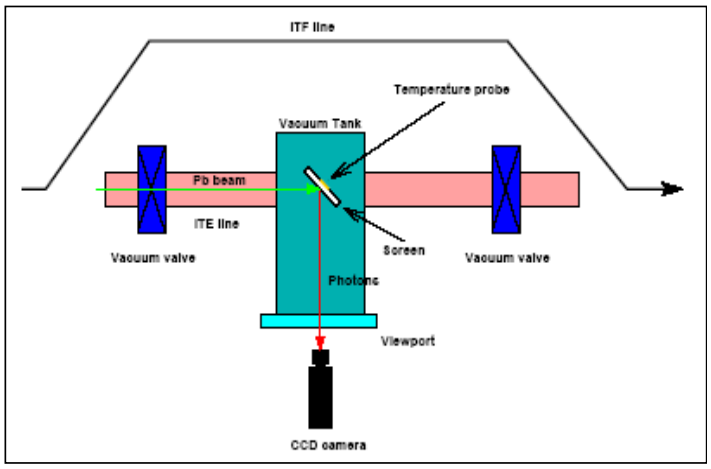

Figure 3-3: Scintillating screen assembly

3.2 **Scintillating screens**

Scintillating screens were used in cosmic ray experiments even before the invention of particle accelerators and have been in common use ever since. It is their simplicity, low cost and power of conviction, which makes them so attractive. A measurement can hardly be more intuitive than to see a beam spot right in the centre of a scintillation screen. In its simplest form, a plate of scintillating material with a graticule printed on it, is inserted into the beam under an angle of 45^0. Through a viewport, located at 90^0 with respect to the beam, a camera observes the screen. Often a second viewport is used to illuminate the screen such that the graticule can be seen.

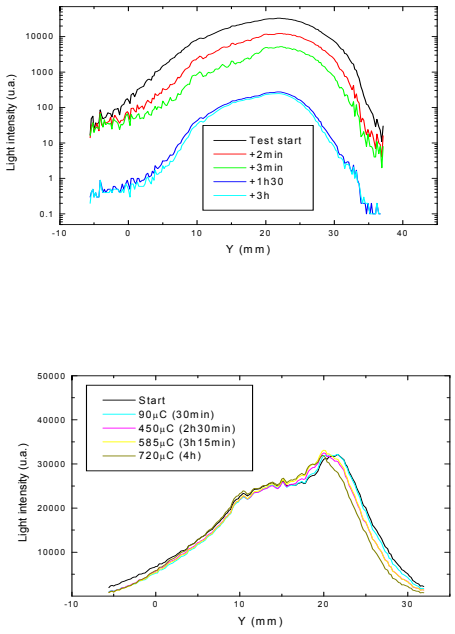

Figure 3-4: Light emission efficiency after bombardment with ions (top: Al2O3, bottom: ZrO2)

At low energies and low intensities the radioactivity induced in the accelerator environment is low enough to use cheap commercial CCD cameras. At higher intensities however the CCD chip will quickly be destroyed through radiation.

Material	ρ *g/cm3*	C_p *at 20°C J/gK*	*k at 100°C W/mK*	***Tmax*** *°C*	*R at 400 °C Ω.cm*
Al2O3	3.9	0.9	30	1600	10^{12}
ZrO2	6	0.4	2	1200	10^{3}
BN	2	1.6	35	2400	10^{14}

Table 3-1: Scintillating material properties

In this case Nuvistor based cameras are used. Also, cheap lenses turn brown under radiation and must be replaced regularly. The same is true for the viewports.

As we have already seen during the discussion of Faraday Cups, the deposition of energy and charge in the intercepting material may lead to heating problems and electrical charging and may even destroy the detector. To ensure that the screen used at CERN's ion facility will survive bombardment with lead ions, several scintillating materials have been tested in the beam. The scintillating material was exposed to 4 MeV/u lead ion pulses of 50 µA and 200µs at a pulse rate of 5 Hz. While Al_2O_3 (chromox) screens showed an important decrease in their scintillating efficiency, ZrO_2 screens turned out to be more stable (see Figure 3-4). Cromox screens are largely used in higher energy proton machines and were used as reference, Even though the ZrO_2 screen had been clearly affected by the impinging beam, its scintillation properties remain unchanged.

Figure 3-5: Alteration of the screen of exposure to ion beams

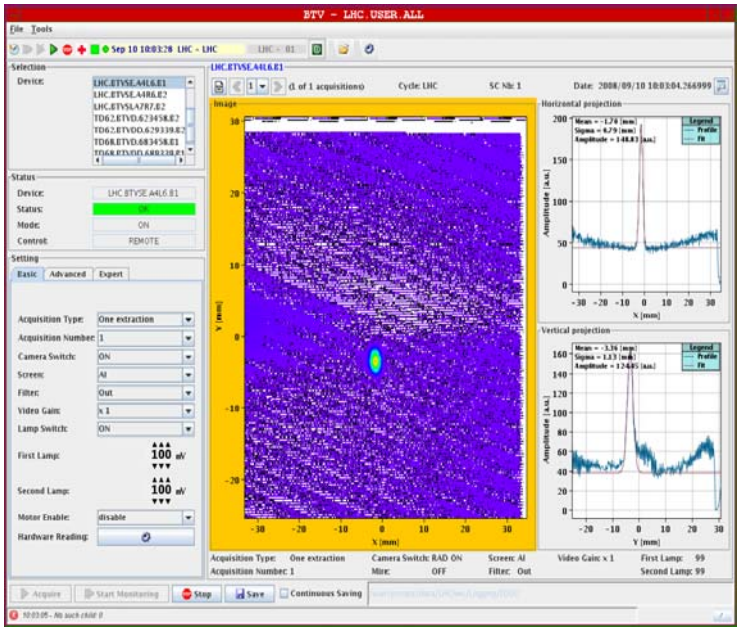

Figure 3-6: TV application program at the LHC

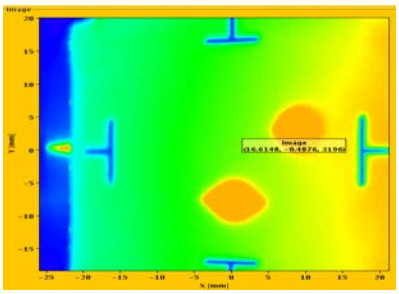

Figure 3-7: First turn in the LHC

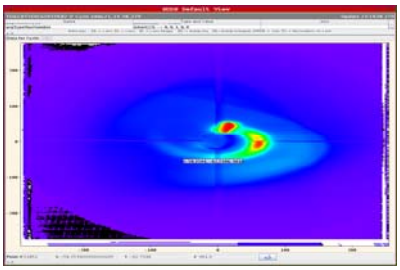

Figure 3-8: Beam spot at the LHC beam dump

In order to get a more qualitative picture than the furtive glimpse onto a quickly disappearing beam spot, the video signal from the camera can be digitized with a *frame grabber,* keeping the digitized image in a frame memory. This converted image may then be used to either re-create a video signal, allowing observation until the next beam pulse passes, or it may be read out by a computer for further data treatment as has been done for Figure 3-6.

Scintillating screens were the main instruments used during the press day at CERN, when the first turn of a particle bunch in the LHC was attempted. First a screen was inserted into the machine at the injection point showing the injected beam. Then this screen was retracted and another one, further downstream was inserted, thus following the beam step by step through the machine. Once a full turn was attempted, 2 spots could be seen on the screen corresponding to the 2 turns (Figure 3-7).

In order to avoid hitting the beam dump with the full beam in a single spot the beam is guided in a spiral way using fast magnets. This can be seen in Figure 3-8.

3.3 **In/Out Mechanisms**

Sensors being inserted into or traversing the beams often require complex mechanical assemblies. The sensor position must be precisely known and often the device must be inserted and extracted in a very short time (some 200 ms). This leads to a multitude of different assemblies, driven by electric motor (dc motors, ac motors or stepping motors are all in use) or by pneumatic systems, both, linear and rotating. Figure 3-9 and Figure 3-10 give a few examples.

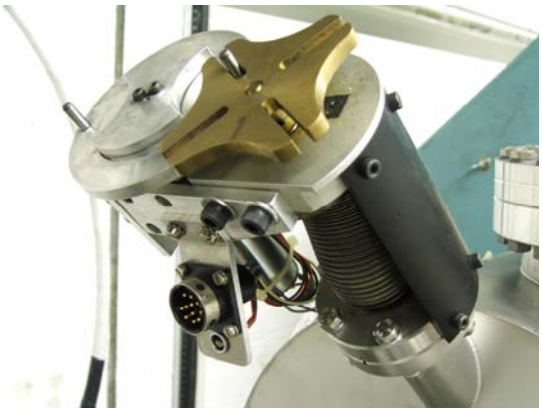

Figure 3-9: Rotary in/out mechanism with electric motor for 4 positions

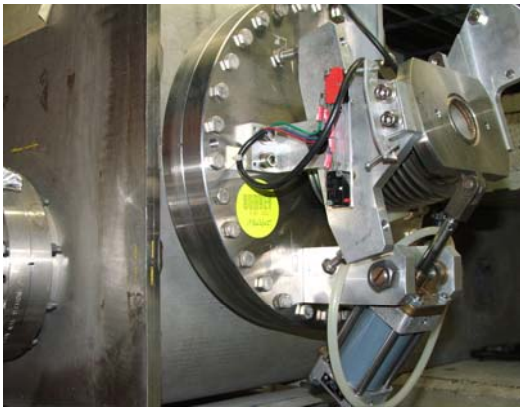

Figure 3-10: Pneumatic in/out mechanism

3.4 **Secondary Emission detectors**

In order to measure the transverse distribution of the particle beam, a wire array or a set of very thin metal ribbons is inserted into the beam. By interacting with the wire material, secondary electrons are emitted and a voltage potential is created. This results in a current flowing back onto the wire which is amplified and measured. The ejected electrons are collected through clearing fields, created by a polarization voltage of some 100 V, avoiding the build-up of an electron cloud on the surface of the wires. Figure 3-11 shows a secondary emission grid with its clearing electrodes (diagonal wires). Since each wire delivers a signal proportional to the number of particles hitting its surface, a beam profile, the projection of the particle density distribution, can be determined.

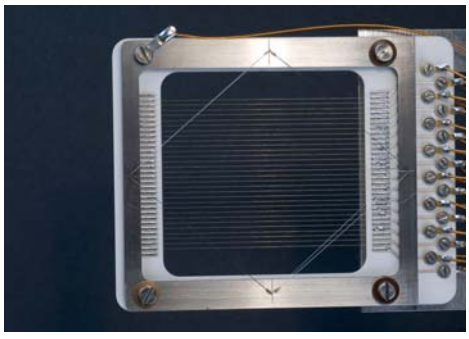

Figure 3-11: Secondary Emission grid

3.5 **Wire Scanners**

When trying to measure beam profiles in circular machines the secondary emission grid cannot be used. Firstly, the beam blow-up caused by the scattering of the beam particles in the wire material will falsify the measurement and secondly, multiple passages of beam particles will deposit thermal energy, which will cause the destruction of the SEMgrid wires for any beam of reasonable intensity.

(SEMgrids have been used in circular machines for the measurement of emittance matching, measuring profiles on multiple turns but only some 20 consecutive profiles were taken into account, limiting the blow-up effect and dumping the beam after these 20 turn in order to spare the detector).

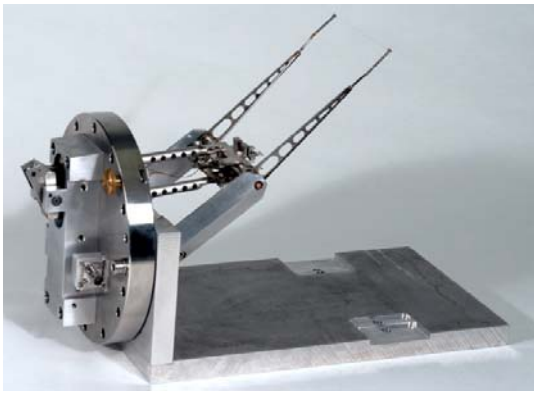

Figure 3-12: Fast wire scanner

Figure 3-13: Fast wire scanner with scintillator and photomultiplier

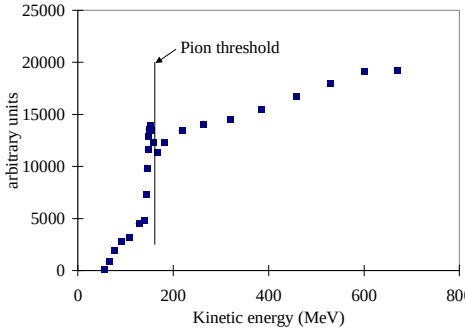

Figure 3-14: Pion threshold for the production of secondary particle showers

A wire scanner consists of a thin straight wire of light material, often SiC or Carbon which is passed through the beam. This limits the energy deposition in the wire (Bethe Bloch:

$$\frac{dE}{dx} \propto \rho \frac{Z}{A}).$$

If the beam energy is high enough a secondary particle shower is created which is detected by a scintillator-photomultiplier assembly outside of the vacuum chamber.

In order to limit beam blow-up and to avoid measurement errors, due to adiabatic damping (see Figure 3-12) and current increase due to change of the revolution frequency when measuring during acceleration, the wire speed must be as high as possible. Currently speeds or up to 20 m/s have been achieved.

At beam energies below 150 MeV, the minimum energy needed to create pions, hardly any secondary particles are seen on the scintillator.

If however the wire is mounted electrically isolated, the secondary emission current from the wire can be measured. In this case, the low energy of the primary beam particles is not an issue. As Figure 3-15 demonstrates, very clean profiles can be measured with secondary emission, while the photo-multiplier signal becomes very noisy and asymmetric due to geometrical effects depending on the placement of the scintillator.

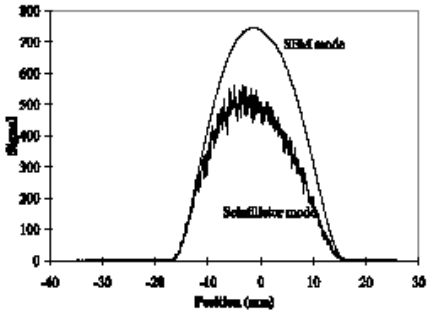

Figure 3-15: Profiles at low beam energy

Profiles of partially stripped ions cannot be measured with such a wire scanner because the interaction of the ion with the wire will induce stripping (one or more electrons will be removed from the ions atomic shell) and the ion will be lost.

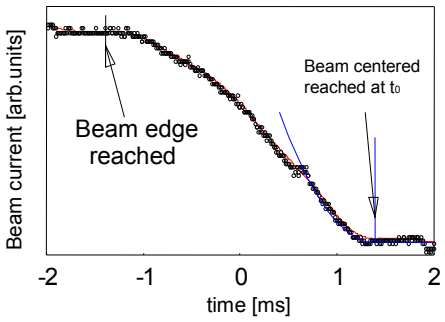

Figure 3-16: Betatron amplitude distribution

One can however use the stripping effect to measure the betatron amplitude distribution. In this case the wire scanner (or a scraper) is used to scrape off the beam starting from the outside of the particle distribution and finishing as soon as the core of the beam has been reached. The losses are observed on a DC current transformer. Figure 3-16 shows a typical loss curve from which the amplitude distribution and the intensity profile can be determined.

3.6 **Transverse Emittance Measurements**

In a circular machine the beam emittance is related to the beam size by the formula

$$\varepsilon_x = \frac{1}{\beta_x(s)}\left[\sigma_x^2 - \left(D(s)\frac{\Delta p}{p}\right)^2\right] \qquad \text{and} \qquad \varepsilon_y = \frac{\sigma_y^2}{\beta_y(s)}$$

The beta function ($\beta_x(s)$) at the position of the measurement as well as the dispersion function (D(s)) must be known or measured separately. The emittance then depends only on the beam size σ_x which can be measured e.g. by a wire scanner. Figure 3-17 shows an example from the LHC wire scanner.

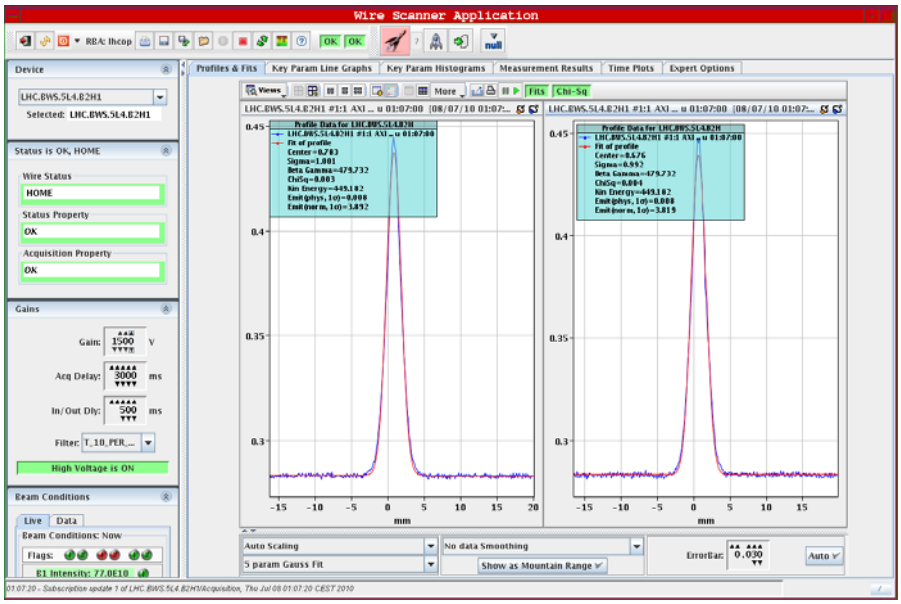

Figure 3-17: Results from the LHC wire scanner

3.7 **Phase Space Scanners**

Emittance measurements at low energies are often accomplished with slit and grid devices. These devices allow scanning the transverse phase space by moving the slit through the beam, where each slit position defines a vertical slice in phase space. For each slit position the angular distribution of the beamlet passing the slit is measured with a secondary emission grid (SEMgrid). Since the time it takes to perform a full scan of the phase space is determined by the number of slit movements and the duty cycle of the Linac, which at CERN pulses every 1.2 s, a measurement can easily take a minute to perform.

In order to be able to scan the full phase space within a single Linac macro pulse of 100 µs, 2 kicker magnets are used to sweep the beam in a parallel manner in front of the slit instead of mechanically moving the slit through the beam. Figure 3-18 shows the measurement line as well as the movement of the particles in phase space along the line.

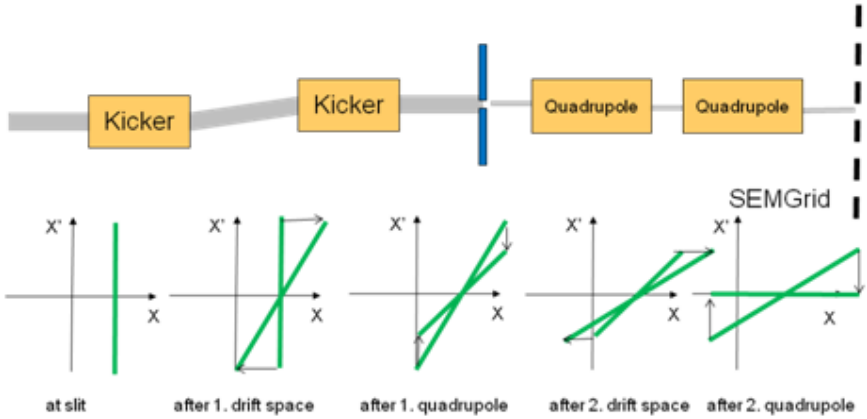

Figure 3-18: Single shot phase space scan

The scaling of the two horizontal (position axis) is determined by the kicker pulse amplitude while the scaling of the y axis can be controlled through the 2 quadrupoles. The surface of the ellipse determines the emittance while the Twiss parameters can be determined from its orientation. The Twiss parameters are used to control the matching of the Linac beam to the acceptance following synchrotron. Figure 3-19 shows a typical measurement result.

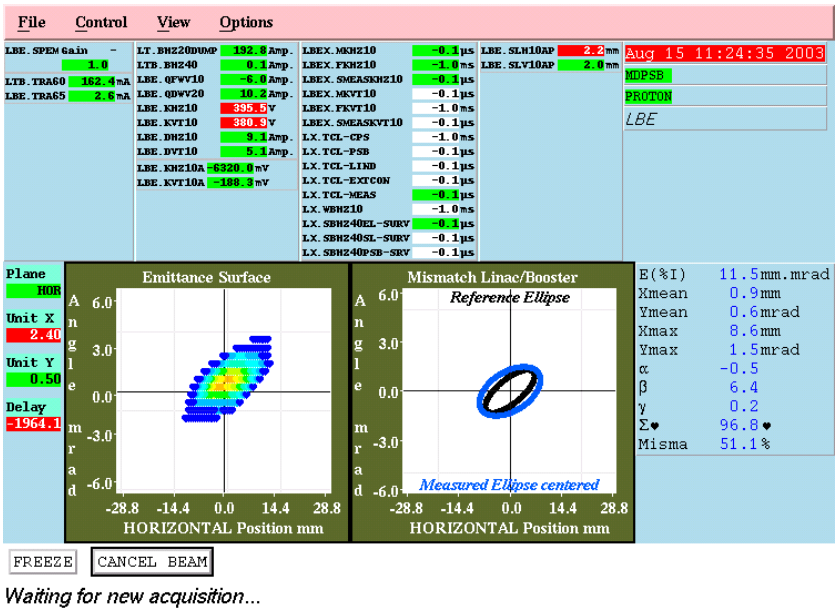

Figure 3-19: Results from single pulse emittance measurement

3.8 **Adiabatic damping**

When a beam is accelerated, its emittance shrinks due to adiabatic damping. This effect can easily be visualized: The particle's velocity component in forward direction is increased, which results in smaller transverse displacements at the same longitudinal distance. The normalized emittance $\varepsilon_{norm} = \varepsilon_{physical}\beta\gamma$ (with β: particle speed and $\gamma = \frac{1}{\sqrt{1-\beta^2}}$: Lorentz factor) however is constant under ideal acceleration conditions.

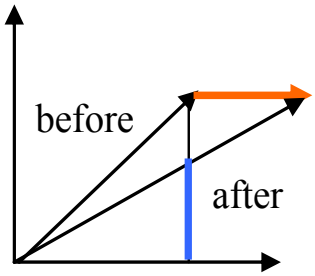

Figure 3-20: Adiabatic damping

4. LONGITUDINAL EMITTANCE

Just like the transverse emittance, determined by the distribution of particle positions and angles a longitudinal emittance, determined by particle energies and phase angle (or time of arrival) can be defined. While direct measurements of transverse emittance are rather common, direct measurements of longitudinal emittance are much rarer. Usually only a spectrometer followed by a profile measurement device allows determining the energy distribution. At the CERN proton Linac a measurement line has been built which uses a clever method to measure longitudinal emittance directly.

The energy distribution is first converted into a horizontal angle distribution which is swept in front of a slit. The slit selects an energy slice whose phase distribution must be determined. This is done by passing it through a buncher, which transforms the phase distribution to an energy distribution which in turn is analyzed by a second spectrometer magnet and measured with a SEMGrid. Plotting the phase distribution for each energy slice allows visualizing the longitudinal phase space distribution directly.

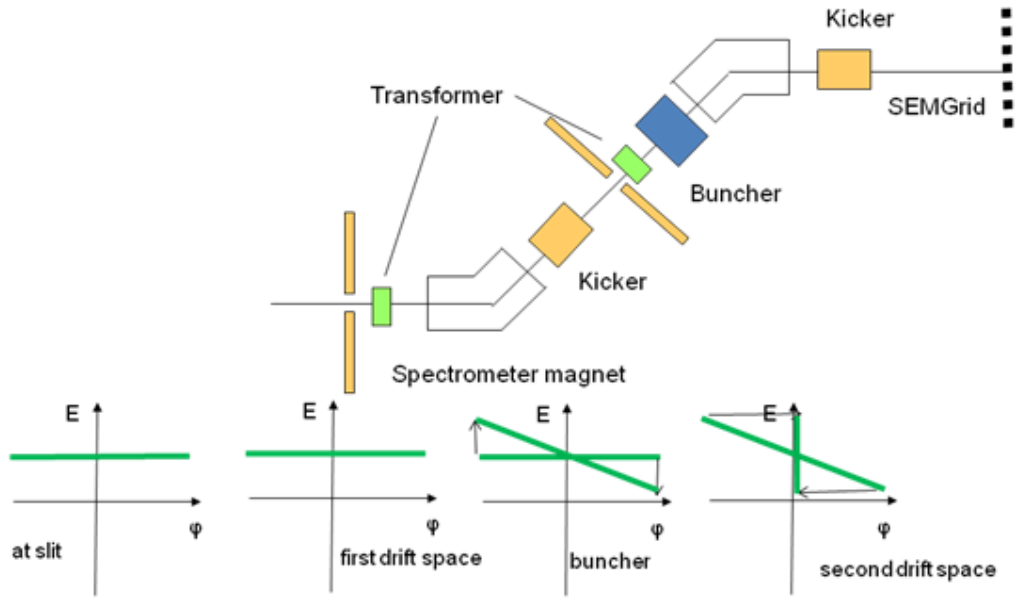

Figure 4-1: Longitudinal emittance measurement

5. PHASE SPACE TOMOGRAPHY

Consider a circular machine with a single RF cavity for acceleration, powered with a sinusoidal accelerating field. Synchronous particles having exactly the correct phase with respect to the RF field will get the pre-determined energy increase while particles coming early will be accelerated less and particles coming late will be accelerated more. This results in a movement in phase space shown in Figure 5-1. The longitudinal profile, measured with e.g. with a wall current monitor, corresponds to a projection of the phase space distribution onto the Φ axis.

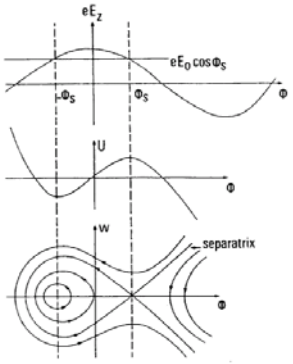

Figure 5-1: Longitudinal Phase Space

Observing the bunch profile for many turns in the machine corresponds in fact to making projections onto the Φ axis "rotating" around the phase space distribution.

Medicine uses similar measurements to visualize 3-dimensional structures in the human body. Many X-ray images are produced with an x-ray camera rotating around the patient's body. The 3-dimension object is re-constructed using Algebraic Reconstruction Techniques (ART).

Figure 5-2: Computer tomography scanner

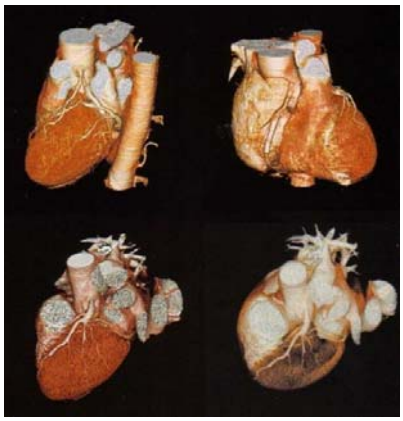

Figure 5-3: Heart tomography

The principle is rather simple (the implementation however can be rather complex and requiring a lot of computing power): The x-ray image, which is in fact a projection of the 3-dimensional object onto the camera axis, is back-projected. Doing this for many images allows the re-construction or the original object. Projecting the reconstructed object and comparing this with the result of the projection from the original object allows correcting the errors. This can be done iteratively.

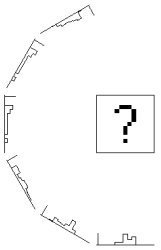

Figure 5-4: Projection

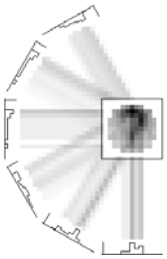

Figure 5-5: Back Projection

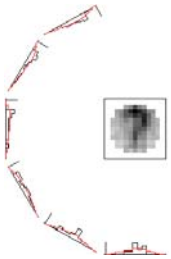

Figure 5-6: Difference projection – back-projection

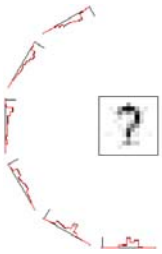

Figure 5-7: After 50 iterations

The method of ART can be applied to the profiles obtained from wall current monitors measuring bunch profiles over many turns. While the individual measurements do not exhibit any detailed phase space information, the reconstructed phase space plot display a wealth of interesting details which cannot be observed otherwise.

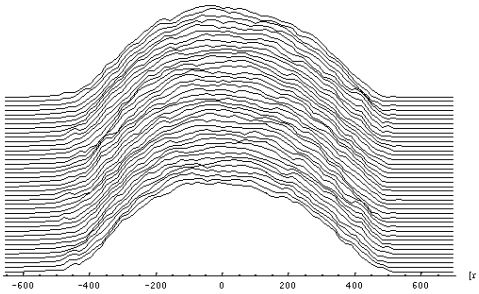

Figure 5-8: Bunch Profiles

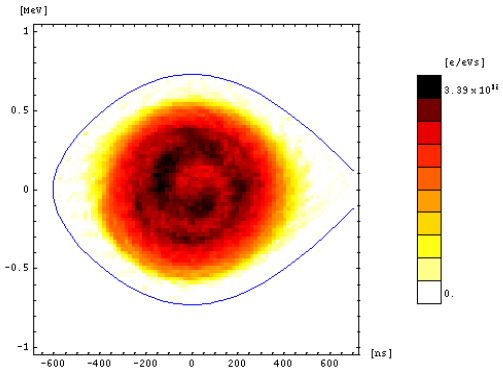

Figure 5-9: Reconstructed longitudinal phase space

6. POSITION MEASUREMENTS

6.1 Beam position monitors

In order to measure trajectories through a transport line or beam orbits in a circular machine, beam position monitors (BPMs) are needed. These devices make use of either the beam's electric or magnetic field and exist in a large variety. Since they pick up the beam's fields they are also commonly called *pick-ups*.

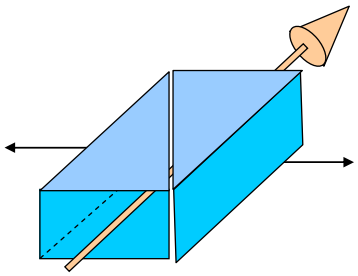

Figure 6-1: Shoebox pickup

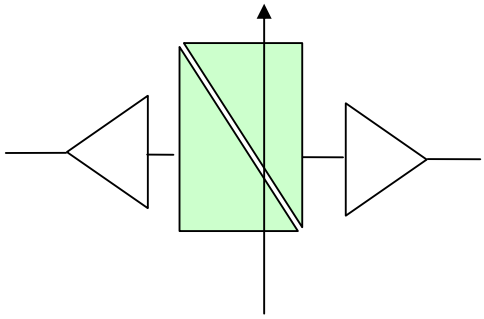

Figure 6-2: Inducing charges on an electro-static pick-up

An electro-static pick-up (coupling to the beam's electric field) is shown in Figure 6-1. We call it shoe-box pick-up because its form resembles a shoe-box which is diagonally cut into 2 halves.

If a beam passes with a certain average displacement with respect to its nominal central orbit, it induces a different amount of charge on each of the two halves. Since the box is cut in a linear fashion, the position can easily be calculated: $x \propto \frac{U_L - U_R}{U_L + U_R}$ where U_L-U_R is often called the Δ signal and U_L+U_R the $\sum$ signal.

Figure 6-3: Cylindrical pick-up

Many ingenious cuts have been invented in order to measure horizontal and vertical positions with a single device.

If instead of a box type pick-up a cylindrical geometry is chosen, the electrodes have a more complex form, but the Δ signal can still be made linear with the beam displacement. Cutting a cylinder diagonally and then unfolding it results a sine curve. If the negative part of the sine is flipped (|sin(x)|) then a V-cut will result and one can create horizontal and vertical electrodes. The pick-up in Figure 6-3 can measure positions in both planes (there are 4 electrodes) and is perfectly linear with displacement, as can be seen in the calibration measurement of Figure 6-4.

Figure 6-4: BPM calibration measurement

6.2 **Trajectory measurement at LHC**

When the LHC was first switched on and particles injected, their trajectory was measured and the orbit immediately corrected, using the known theoretical optics of the machine and taking into account the measurement which includes alignment errors and magnet errors. Figure 6-5 shows the particle orbit when it was only partially corrected. Big excursions can be seen to the right of the plot. Once the orbit was corrected the particles were able to make a first full turn.

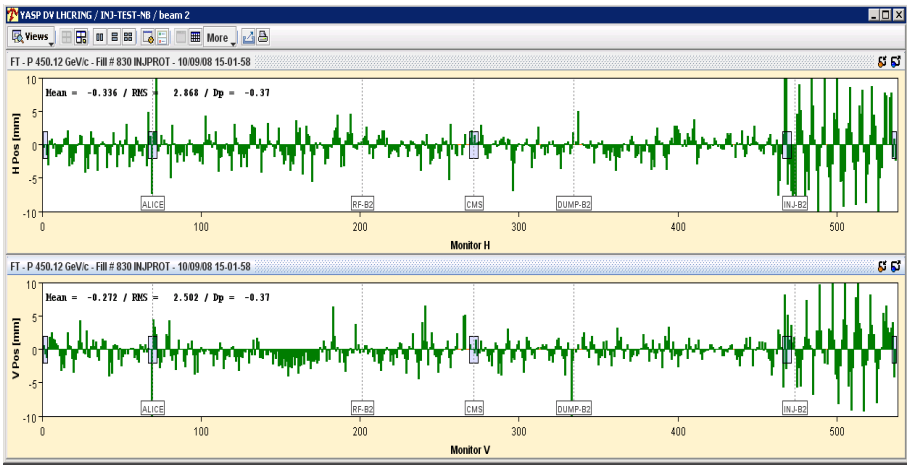

Figure 6-5: LHC trajectory measurement and orbit correction

7. TUNE MEASUREMENTS

7.1 What is the machine tune?

When a particle is not exactly on its design orbit it will not pass through the centre of the machine's focusing quadrupoles and therefore it will experience a focusing force, which will lead to so-called betatron oscillations. The number of oscillations around the closed orbit is called the betatron tune. This is true for horizontal as well as for vertical displacements. If the number of oscillations corresponds to an integer value, then each small imperfection in the machine will lead to a small kick, which will be repeated each time the particle passes that point. This leads to a (integer) resonance, which will result in the loss of the beam. It can easily be shown that the same is true for half integer tunes and in fact any particle for which $l \cdot Q_h + m \cdot Q_y = r$ holds where Q_h and Q_v are the horizontal and vertical tune values. The tune diagrams show these lines of instability, seeFigure 7-1.

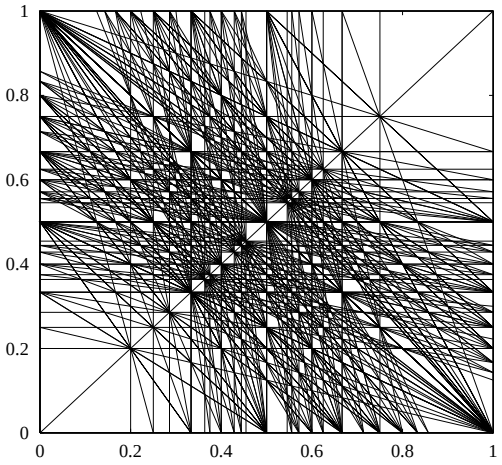

Figure 7-1: Tune diagram

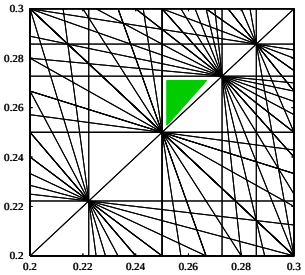

Figure 7-2: Working point in the tune diagram

The machine must operate in a resonance free zone of the tune diagram (the working point) in order to avoid beam blow-up and finally loss of the beam. This shows the importance for a precise determination of the tune values.

7.2 Measuring the tune

In order to measure the tune values, the betatron oscillations must be observed. This can be done by placing beam position monitors all around the accelerator ring and observing the beam trajectory. Since normally the beam circulates on its closed orbit with very small (immeasurable deviations) the beam is usually coherently excited with a kicker magnet. As we have seen in the previous section we are actually only interested in the non-integer part of the tune and this can be measured with a single beam position monitor. In Figure 7-3 you can clearly see that it is not possible to distinguish q from 1-q and that in addition to the base frequency higher harmonics can be fitted to the data measured by the pick-up.

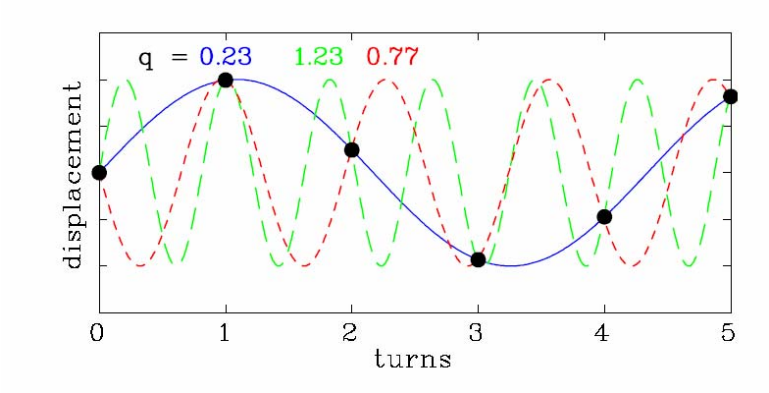

Figure 7-3: Measuring tune with a single pick-up

The measurement at the CERN PS and PS Booster works as follows: The beam is exited with a kicker in short intervals (min 5 ms). The beam position is measured by a pick-up (PU) delivering horizontal and vertical difference signals which are proportional to the beam displacement. The PU is of shoebox type, consisting of a metal box with a diagonal cut. In fact, the PU used here combines horizontal and vertical cuts in a single device with 4 taps to extract the signals from the left/right and upper/lower plates.

A passive hybrid circuit, being virtually insensitive to radiation, is mounted directly on the pick-up (the denominations pick-up (PU) and beam position monitor (BPM) are used interchangeably). The hybrid combines the signals from the PU plates and converts them to difference (Δ) and sum (Σ) signals.

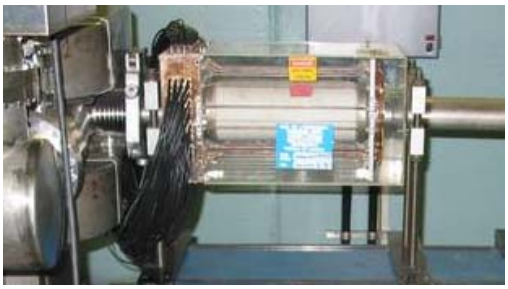

Figure 7-4: The tune kicker

During acceleration the beam may undergo slow but rather large closed orbit variations which are filtered out by a Beam Orbit Signal Suppressor (BOSS).

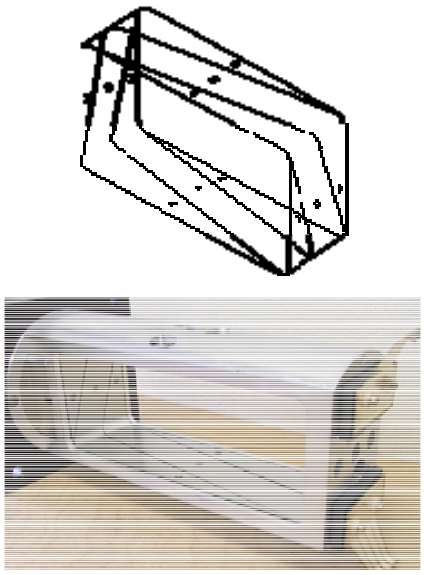

Figure 7-5: Pick-up electrodes

Figure 7-6 shows the architecture of the readout electrons at the PS Booster. The Booster actually consists of 4 vertically stacked synchrotrons. The MUX is used to select the position signals from any of the 4 Booster rings. The difference signal is not only proportional to the displacement but also to the beam intensity, which may vary by several orders of magnitude. This is taken care of by a gain controlled Amplifier (GCA). The signal is converted to digital values with a 14 bit ADC and 2048

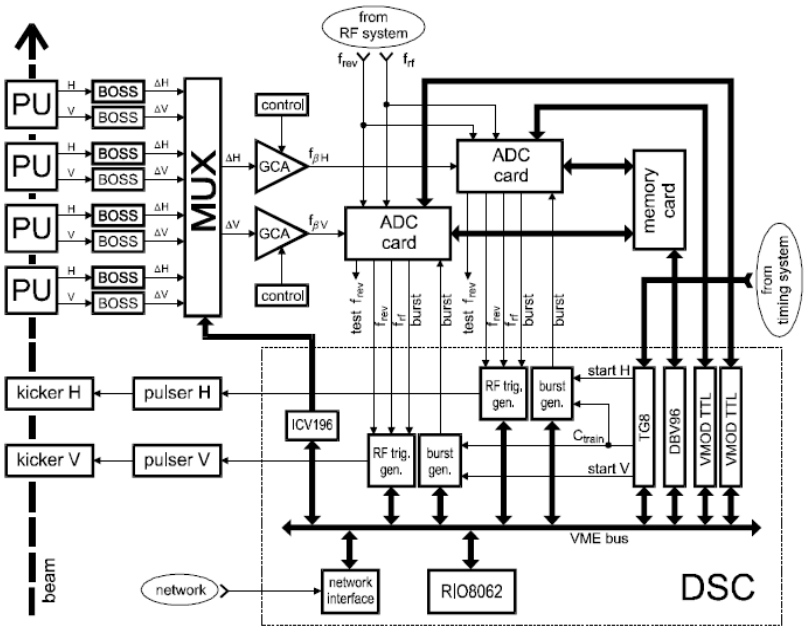

Figure 7-6: Tune measurement electronics

converted values are stored in a memory card. A digital signal processor card (DBV96) with a Motorola 96002 Digital Signal Processor accesses these data over a dedicated high speed memory bus.

The results are stored in DSP memory and can be transferred to the VME processor through a communication mailbox implemented in the DSP. From there the results are transferred over the local area network to the operator consoles in the control room for visualization.

7.3 **Calculating the tune**

As can be seen from Figure 7-3 the frequency of the measured signal is related to the revolution frequency and the oscillation mode through

$$f_\beta = (m \pm q) f_{rev} \qquad (1)$$

where m is the integer number of oscillations and q is the non-integer part of the tune. Since the integer part of the tune stays constant only q needs to be measure. This reduces the equation to

$$\frac{f_\beta}{f_{rev}} = q \qquad (2)$$

As already mentioned, the closed orbit is not centered and stable during acceleration which results in an additional component of the revolution frequency in the signal. A convenient way to calculate q is to sample the PU signal at a rate proportional to the revolution frequency and to perform FFT analysis on N samples. Using a sampling rate of $k*f_{rev}$ (k is the over-sampling ratio) q can be determined by

$$q = k \frac{n_\beta}{N} \qquad (3)$$

where n_β is the bin number in the FFT spectrum.

7.4 **Data handling**

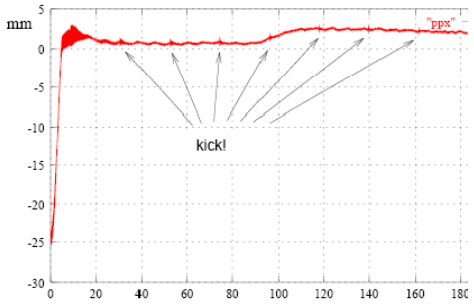

Figure 7-7: Kicking the beam

After starting the measurement the beam is kicked and 2048 beam positions are measured and stored in a dedicated memory card. These data are transferred to the DSP and the memory is again freed to take new data. Through this double buffering data can be taken while the previous batch is processed by the DSP.

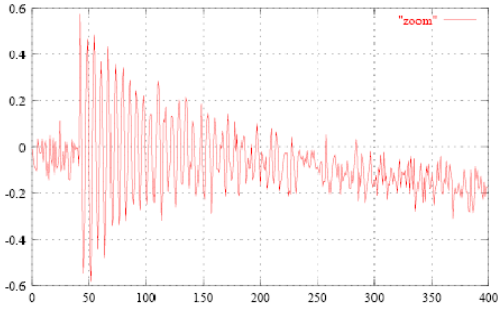

Figure 7-8: Zoom of the kick

The Fourier transform expects a signal that constitutes one cycle of a periodic signal. Since our signal is cut out of the stream of oscillations in an arbitrary manner, discontinuities occur when extending it to a periodic wave form.

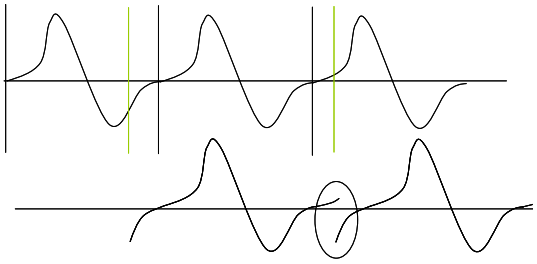

Figure 7-9: Periodic extension of the position signal

This phenomenon can be corrected by windowing. Each value is multiplied by a coefficient which approaches zero at the edges of the window. Typical windowing functions are shown in Figure 7-10. For the tune measurement system the Blackman Harris function is used. The values are pre-calculated and stored as coefficients in a table at initialization of the DSP.

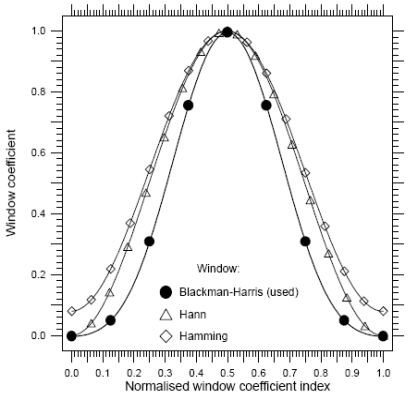

Figure 7-10: Windowing functions

For the calculation of the Fourier spectrum a 1024 point complex FFT is used, followed by an algorithm to extract the real signal spectrum from the complex spectrum data.

From the Fourier spectrum the q value must be found through a peak search routine. Since the over-sampling ratio in equation (3) amounts to 4 only a quarter of the power spectrum needs to be looked at. Q can only take only values between 0.1 and 0.5 which means that the search is limited to a window of 50 and 256.

The peak search algorithm first looks for the for bins for which

the power value V^2 is bigger than the next value: $V^2(n-1) < V^2(n)$

the power value V^2 is bigger than the following value: $V^2(n+1) < V^2(n)$

the power value satisfying the first 2 conditions is the biggest in the observed range

the power value is at least 3 times as big as the arithmetic mean of all power bins. The value 3 has been determined experimentally.

If these conditions cannot be fulfilled then the signal is either too small or the spectrum too noisy.

Most of the mathematics code for the DSP has been written in the C language except of small parts like the arithmetic mean, which has been implemented in assembler for speed reasons.

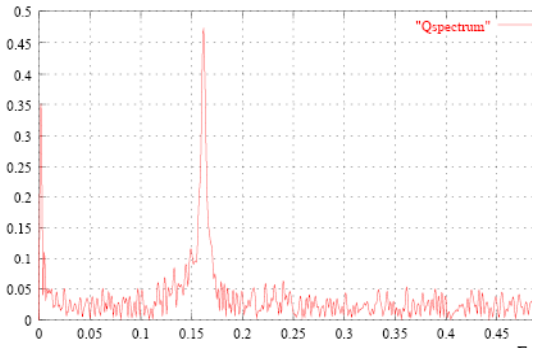

Figure 7-11: The frequency spectrum

7.5 Spectrum Interpolation

When just taking into account the bin in which the peak is found, then the resolution for Q is very limited. In order to improve the resolution one can

Increase the number of points, but this would increase the computing time and therefore slow down the system

Decrease the over-sampling, but this would lead to a degradation to the system input dynamics

Interpolate between adjacent bins.

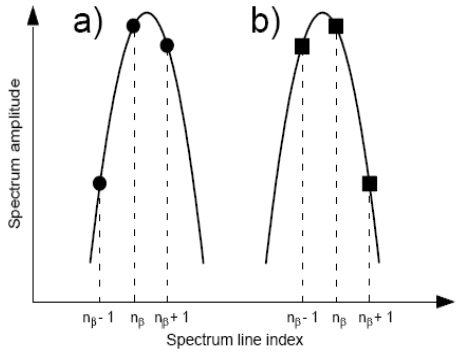

Figure 7-12: Tune value interpolation

Since the betatron frequency spans over several bins, not only due to the discrete FFT but also because the incoming signal is not a pure harmonic but it includes attenuated revolution frequency components, noise etc. Interpolation allows finding the peak position with a resolution better than a bin. The exact form of the peak is unknown but it could be shown that using a parabolic shape, which is easy to calculate, can improve the Q-value calculations significantly.

7.6 Measurement results

During the acceleration cycle the beam is kicked every 5 ms and the Q value is calculated for each of these kicks. A front-end computer reads the results from the DSP and passes them on to an application program in the central control room, where the evolution of the tune during the cycle can be observed in graphical form. The application program also allows controlling the measurement interval, amplifier gains, start of measurement in the cycle and other parameters.

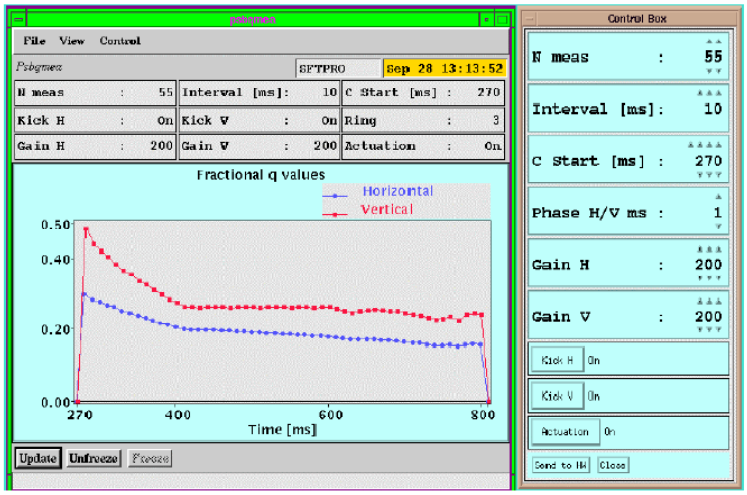

Figure 7-13: Tune measurement results

7.7 Further improvements

As can be seen from Figure 7-8 the position peaks are very sharp because the beam bunch is short with respect to the revolution frequency. As a result the signal power is distributed over many harmonics in the frequency spectrum. By rectifying the signal with a simple diode and capacitor circuit (see Figure 7-14) the signal spectrum can be pushed to the base band and thus the signal power in the tune line to be measured can be significantly increased. This shows that a careful balancing between analogue and digital methods is needed.

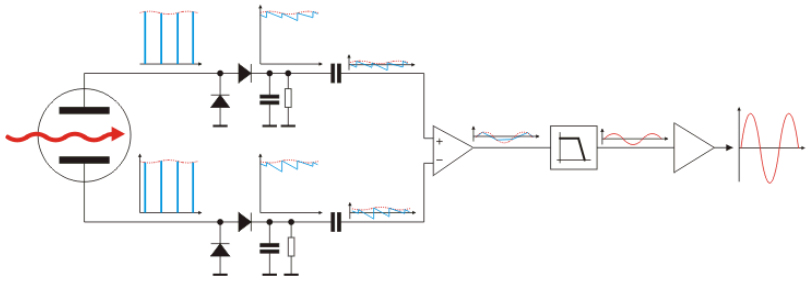

Figure 7-14: Base band Q measurement system

Through this trick it was possible to measure tunes in the SPS without artificial coherent excitation of the beam.

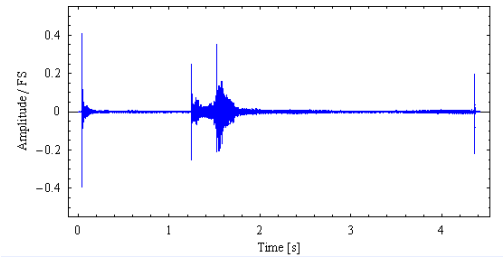

Figure 7-15: Natural beam oscillations

Figure 7-15 shows beam oscillations as they arise during an acceleration cycle in the CERN SPS. The first strong peaks are due to injection, the last peak is created when the ejection kicker is activated. Figure 7-16 shows a waterfall model of the corresponding frequency spectra. It can be seen that the frequencies fall into the audio range which allows using very powerful and cheap audio systems for data acquisition.

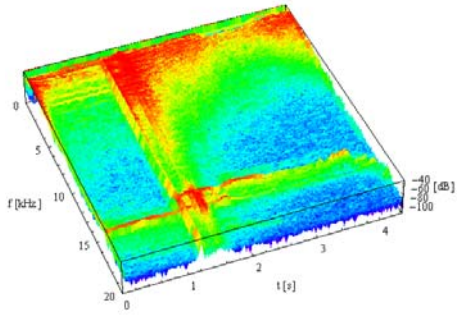

Figure 7-16: Waterfall model of frequency spectra

The tune measurement system described in the previous sections was state of the art some 10 years ago but it is still in operation today. The DSP chip is now obsolete and the software development system consisting of C-compiler, assembler and debugger uses PC hard-and software not available any more.

In the meantime the digital hardware has been replaced and a field programmable gate array (FPGA) has taken the place of the DSP allowing much increased calculation speed. Like this, 128000 data points can be treated instead on the 2048 and Q interpolation will not be needed any more. This shows the common problem that digital hardware and its associated software tools are evolving much faster than the accelerators which have lifetimes of several decencies (the CERN PS was inaugurated in 1955!).

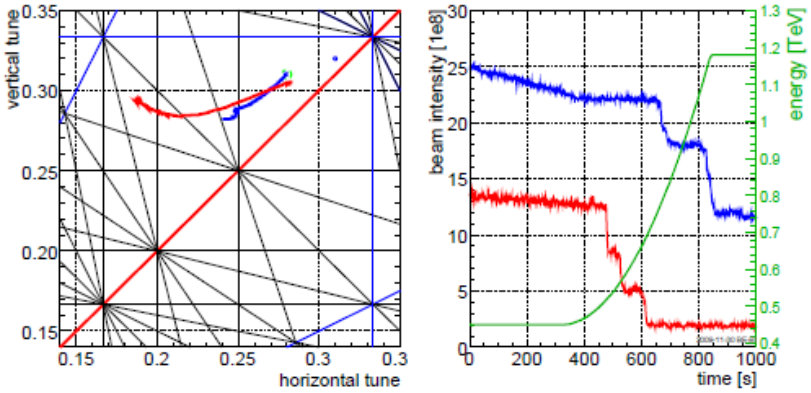

Figure 7-17: Tune changes during ramp and beam losses

7.8 **BBQ tune measurement in the LHC**

During acceleration in the LHC the tunes change such that several basic resonance lines in the tune diagram are crossed resulting in important beam losses. This was expected and immediately noticed during the first acceleration attempt. Figure 7-17 shows on the left how the tunes of the two counter-rotating beams change during acceleration while on the right the corresponding beam intensity is plotted. Losses happen in steps as the resonance lines are crossed.

8. TRAJECTORY MEASUREMENTS

8.1 Trajectories and Orbits

When particles are injected into a circular accelerator, injection errors may occur, resulting in coherent oscillations around the closed orbit. These oscillations may be caused by beam displacement and/or wrong injection angle and may cause emittance blow-up through filamentation. The oscillations can be seen when beam positions are measured turn by turn. When traversing transition (the moment when due to acceleration the orbit radius starts shrinking instead of increasing) the beam may undergo trajectory changes as well as at ejection. Other effects during acceleration may also influence the trajectories. For this reason it is desirable to be able to measure beam trajectories at any time during the acceleration cycle.

In contrast to the beam trajectory, the beam orbit is the average beam position over several turns in the machine. During acceleration the orbit may move considerably and beam losses may occur due to aperture limitations. It is therefore important to be able to measure the orbit all along the acceleration cycle.

8.2 Synchronisation

In order to measure beam trajectories it is necessary to have a big number of BPMs in the machine evenly distributed along the accelerator ring. In the CERN PS there are 40 PUs while in LHC several thousands will be installed. Since the accelerator can treat several particle-bunches (depending on the RF frequency) at the same time, each bunch must be measured turn by turn and the position data saved for the whole accelerator cycle. Another, however less flexible method, is to define the time interval during the acceleration cycle we are interested in beforehand and save the data only for this interval.

For low energy accelerators, where the particle has not yet reached the speed of light, the acceleration will result in a speed increase and therefore in an increase of the revolution frequency. This means that the integration gate, needed for integration of the BPM's Σ and Δ signals must be continuously adapted to the revolution frequency. The current trajectory measurement system installed in the PS can measure 1 bunch during 2 turns every 5 ms and has a very complex synchronization system associated to it, following the revolution frequency in order to generate the integration gate supplied to the ADC.

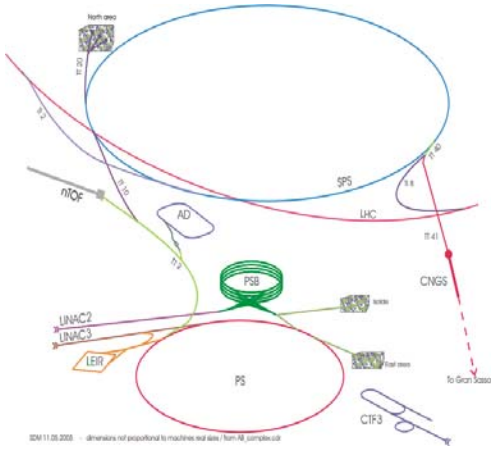

Figure 8-1: Different beams in the PS

In order to complicate things further, the RF harmonic number (the number of RF cycles per revolution, which is equal to the maximum number of bunches that can be accelerated) can be modified during the acceleration cycle. This allows the splitting of bunches into several bunchlets or the recombination of several bunchlets into one big bunch. In such a case, the number of integration gates must be changed on the fly.

The CERN control system allows several operators at different operator consoles to access data from the same measurement system. For example, one operator wants to check the orbit at injection, while another one wants to see the orbit at transition and this should be possible for the same accelerator cycle.

As can be seen from

Figure 8-1, the PS can take particles from Linac2 or Linac3 and it can eject particles to experimental areas (East Hall or nTOF), it can create antiprotons for the Antiptoton Decelerator (AD) or it can transfer protons to the SPS for fixed target physics or for injection into the LHC.

For maximum flexibility the PS implements a concept called *pulse to pulse modulation* (ppm) which allows assembling a series of different acceleration cycles into a so-called super-cycle which is repeated. At any moment it is possible to add or remove any of the individual acceleration cycles using a super-cycle editor. Like this several *users* can use the machine at the same time, everybody getting a few time slices of the global beam time.

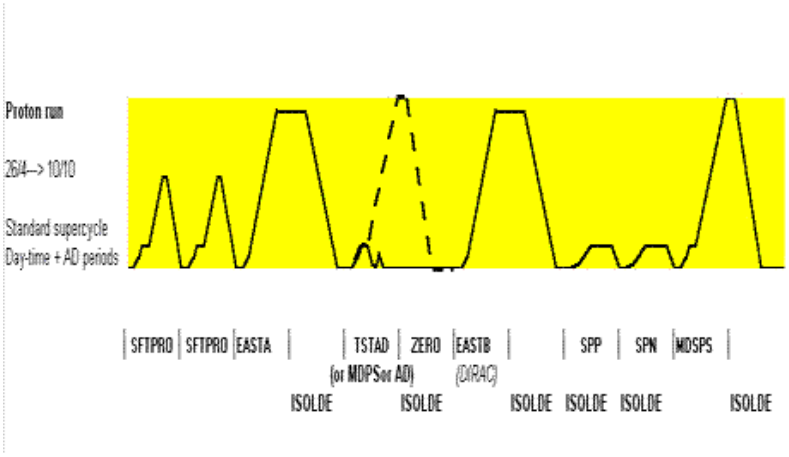

Figure 8-2: The PS super cycle

Figure 8-2 shows a typical super cycle. For low proton energy the cycle time in the PS is 1.2 s while for high energy the cycle time is doubled. For these cycles the Booster may accelerate 2 cycles where the one acclerated during the time the PS is busy is extracted from the Booster directly to ISOLDE. The first text line under the cycle diagram denotes the cycles in the PS (SFPRO, EASTA, LHC …) while the second line shows additional cycles in the PS Booster.

The consequence of this flexibility is the fact that the trajectory measurement system must deal with a great variety of different types of beams:

- EASTB: a single bunch on h=8
- AD: 4 bunches on h=8
- LHC: 4 bunches on h=7, 2 additional bunches are injected on a consecutive Booster cycle
- SFTPRO: 8 bunches fill all buckets on h=8

- EASTC: A small bunch is injected into the first RF bucket, a second, much more intense bunch is inject into bucket no. 7.
  The intense bunch is ejected at 14 GeV. The small on is further accelerated and extracted to a different area later in the cycle.

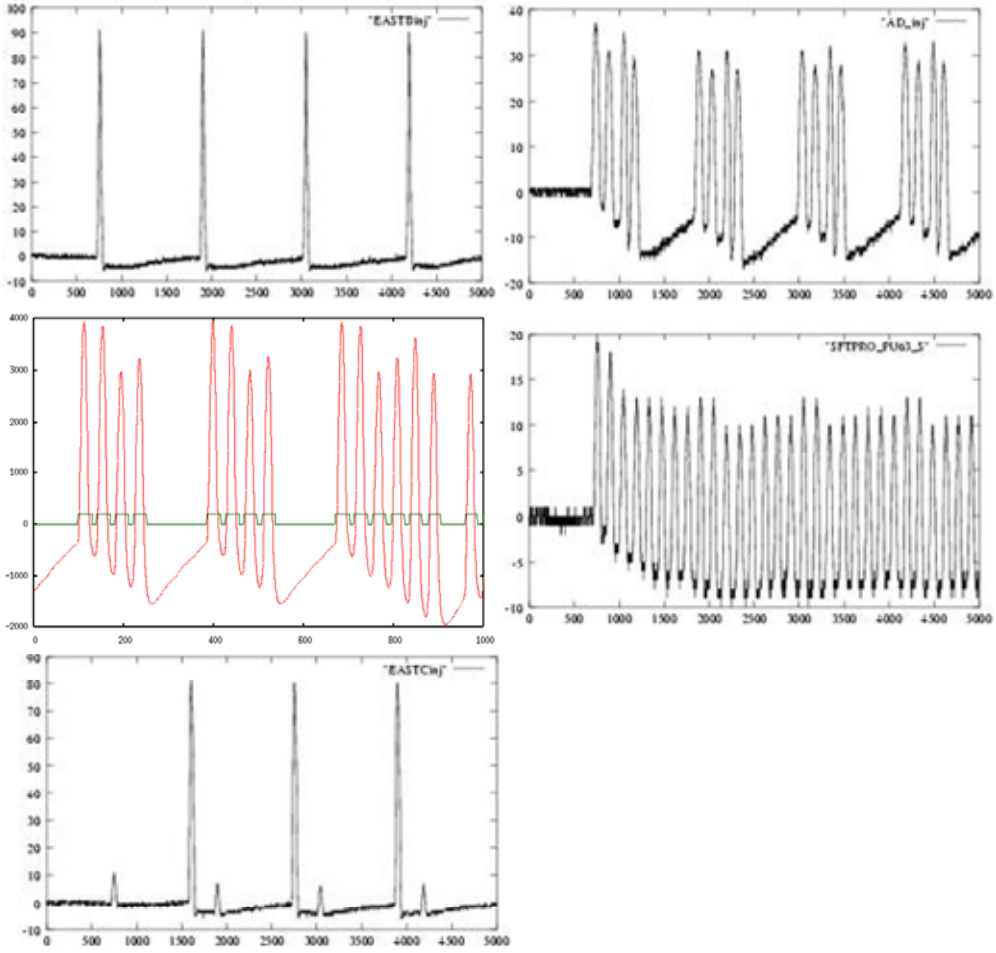

Figure 8-3: Beam types in the PS

8.3 **Readout Requirements**

In order to provide trajectory data at any time within the acceleration cycle, the bunch positions must be calculated turn by turn, from injection into the machine until ejection. This can be done by simply sampling the Σ and Δ signals coming from each BPM in the machine, fast enough to numerically integrate them and subsequently calculate the position from the integration results. It is by far easiest to use a fast sampling clock, asynchronous to the revolution frequency. With a bandwidth

of the pre-amplifiers located near the BPMs of 30 MHz and expecting at least 4 samples for a 30ns bunch, we need a sampling frequency of 120 MHz. Since an acceleration cycle in the PS can take 2s, we need at least 300 MSamples per signal and therefore a total of 8 * 3 * 2 * 300Mbytes (8 bunches, 3 signals per pickup, 2 bytes per sample).

From these quick calculations it can easily be seen that it will be necessary to treat the data on the fly, such that only position data for each bunch and not individual ADC samples are stored. The idea is therefore to use an FPGA to read out the ADC samples, create integration gates synchronous to the bunch frequency on the fly and perform online baseline correction and integration. Figure 8-3 clearly shows how the baseline moves in dependence of the number of bunches and their intensity in the machine.

8.4 **Readout Electronics**

As we have seen in the previous section, the electronics must be capable of

- Reading ADC samples at a rate of ~ 120 MSamples/s
- Synchronizing to the bunch frequency
- Generating the integration gate and numerically integrate the signal
- Finding the baseline and correct for baseline movement
- Storing the integrated and baseline-corrected Σ and Λ signals in a large memory being capable of keeping all values acquired during a 2 s acceleration cycle
- Giving access to the acquired data to the external world

The only way this can be done with today's technology is the use of a fast FPGA associated with big memories.

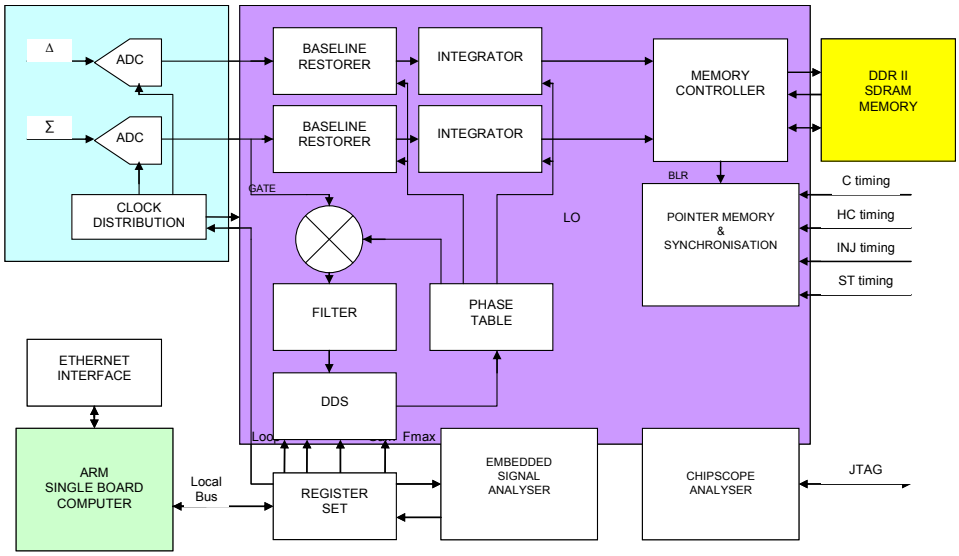

Figure 8-4: Trajectory measurement electronics

Figure 8-4 shows the basic electronics layout. The data coming from the ADC (light blue) block is treated by the FPGA (violet) and stored in memory (yellow). The data can be read out by a single board computer with Ethernet interface.

8.5 **The Algorithms**

In order to develop the algorithms for synchronization, baseline correction and numeric integration for the different types of beams shown in Figure 8-3 the FPGA is first programmed as a chart recorder, sampling passing every sample form the ADC through to the memory. Like this only parts of the acceleration cycle can be recorded but by changing the acquisition trigger any time slice in the cycle can be selected. The acquired data are read out form the memory and stored on files. The algorithms can be developed in MathLab or as offline C programs and can be tested on real data.

8.5.1 The PLL

The basic idea for synchronization is a numerical phase locked loop. The local oscillator (LO) is implemented as a direct digital synthesizer (DDS). The phase of this DDS is compared to the BPM signal and the phase error is filtered and fed back to keep the DDS synchronized. The initial guess of the LO frequency is determined from the measured magnetic field in the accelerator from which the particle energy and thus its speed and revolution frequency can be calculated.

Each incoming PU sample is compared with the phase table to decide if it is part of the signal or part of the baseline. The phase table is simply a circular buffer addressed by the highest significant bits of the DDS phase accumulator. The content of the phase table depends on the harmonic number and is pre-loaded before the start of the acceleration cycle. In case of RF gymnastics (see section 8.7) the phase table must be switched to new values on the fly.

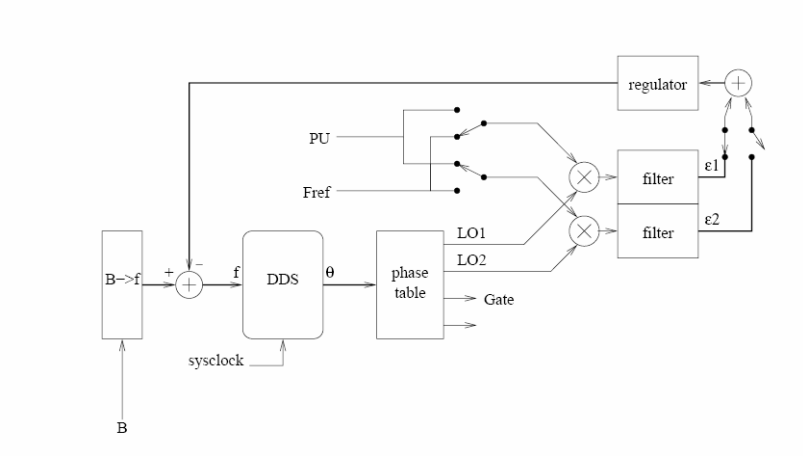

Figure 8-5: Phase locked loop

The problem is similar at injection: Before having beam in the machine there are no signals coming from the PUs. Instead a reference signal coming from the RF system is used for synchronization. Once the beam is circulating in the machine an external timing pulse switches to the new reference frequency.

These algorithms can be easily tested offline on the data taken with the chart recorder.

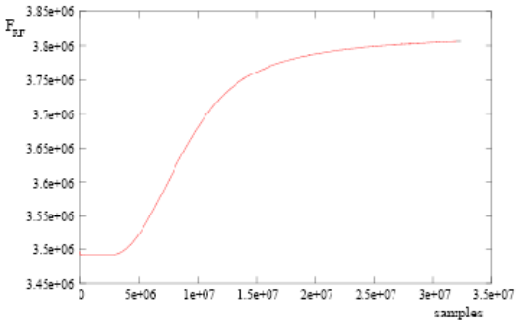

Figure 8-6: Measured frequency swing during acceleration

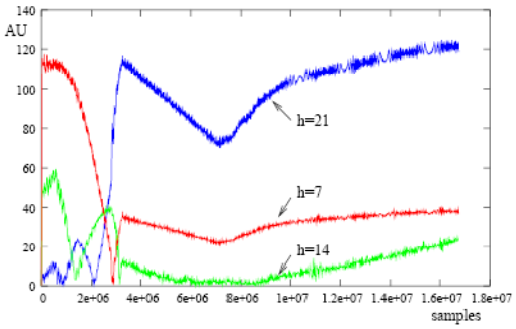

Figure 8-7: Frequency contents during bunch splitting

8.5.2 Baseline correction

The PU together with its load resistance delivers a high-pass filtered, and therefore differentiated version of the beam signal. The base line restorer uses a low-pass filter and therefore an integrator, with the same cut-off frequency as the PU thus compensating the differentiation effect. When integrating however the integration constant is not known and a DC level may be added to the signal. Since we know that this DC level should be zero, a second accumulator is added, which is only active when the ADC sample is part of the baseline, which can be deduced from the synchronization PLL.

8.6 **Algorithm implementation in the FPGA**

In the first, offline approach, the PLL in Figure 8-5 was implemented in a C program. The filter was a second order Butterworth low-pass filter whose coefficients were determined using a Matlab program.

$$H_F = 9.8 \cdot 10^{-6} \frac{1 + 2z^{-1} + z^{-2}}{1 - 1.9911z^{-1} + 0.9911z^{-2}}$$

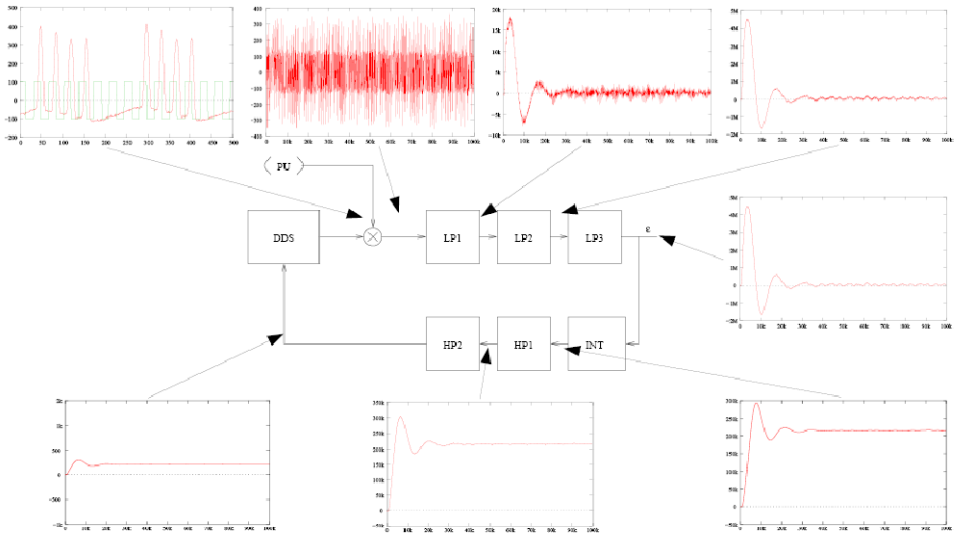

Figure 8-8: Splitting the loop filter

Once implemented in the FPGA the algorithms must be capable of swallowing the data coming from the PU, which means a rate of ~ 120 MHz. Calculating this formula in floating point is simply not feasible. Therefore the algorithm was re-viewed and replaced by a series of low-pass filters followed by an integrator and high pass filters using exclusively integer calculations in such a way that the coefficients can be calculated with a few shifts and additions. By subdividing the filter into several stages pipelining the algorithm in the FPGA becomes possible. Because of the large ratio between sample rate and the dominant system frequencies, a few clock cycles of pipeline delay do not affect the loop dynamics. Once the baseline is corrected and the signal is synchronized, the phase table is used to generate the integration gate. All Σ and Δ samples within the integration gate are added and the results stored in memory. The positions can then be calculated through

$$x = S_x \frac{\Delta_x}{\Sigma}$$

8.7 **Harmonic number changes**

Synchronisation is largely complicated through harmonic number changes. By changing the RF frequency the bunches can be split into several sub-bunches (bunch-splitting) or the distribution of the bunches on the ring circumference may be modified (batch compression).

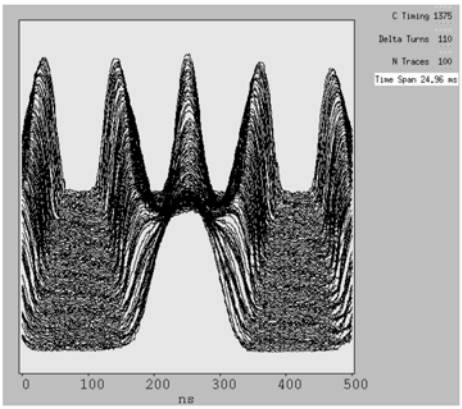

Figure 8-9: Bunch splitting

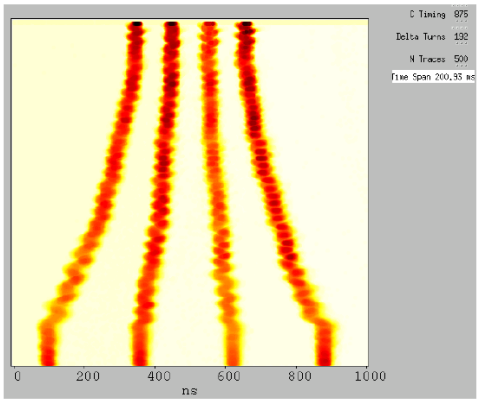

Figure 8-10: Batch compression

The frequency contents of the PU signals during triple splitting (a bunch is split into 3 as seen in Figure 8-9) is plotted in Figure 8-10. At a certain moment, determined by an external timing signal it must be decided to switch from measuring the position of a single bunch to measuring the positions of the 3 bunchlets. This moment corresponds to the crossing of the blue (h=21) and the red (h=7) frequency lines in Figure 8-7.

In order to find back the position in the table of measured Σ and Δ values where the switch has happened, address pointers, linked to these external timing events must be kept in a separate table.

8.8 **Integration**

Last not least the baseline corrected sum and difference signals must be integrated, which is done by simple addition of the samples within the integration gate calculated by the synchronization algorithm.

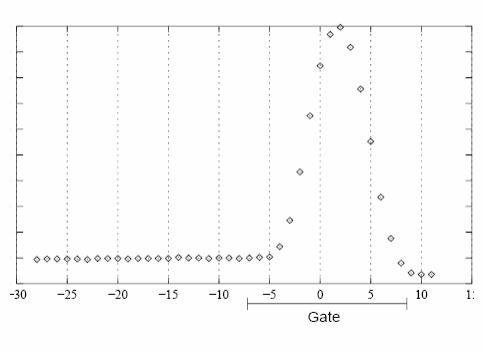

Figure 8-11: Integration

9. MACHINE PROTECTION SYSTEMS

While in low intensity and low energy accelerators the beam cannot do much harm even if the whole beam is lost in the vacuum chamber, this is clearly not the case for high energy and high intensity machines. Already at the CERN Linac, a machine with a top enery of 50 MeV, 160 mA during a 200 μs beam pulse and a repetition rate of 1.2s it it was possible to burn a hole into one of the vacuum joints. How much more critical is the problem in the LHC, where will have 2808 bunches at 7 TeV? People amuse themselves calculating the equivalent kinetic energy of known everyday objects. The energy of single bunch in the LHC at top energy corresponds to a 5 kg bullet at 800 km/h[1] and don't forget that there are 2808 of them in the machine. On the other hand these bunches circulate in a magnetic field which is generated by supra-conducting magnets. The loss of a very tiny fraction of these particles will result in a magnet quench and the loss of a big amount, concentrated in a small volume will result in destruction of the equipment.

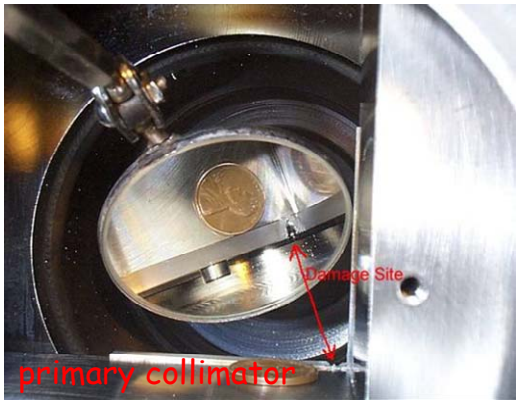

Figure 9-1: Beam damage


Figure 9-2 Ionisation Chamber

At the Tevatron, even though its beam power is 200 times less than the power in an LHC beam, a hole was drilled into the primary collimator (Figure 9-1), when the beam was displaced by 3 mm due to insertion of a movable device, when it was supposed to be out of the vacuum chamber. The secondary collimator was largely damaged and 16 magnets quenched.

9.1 Machine protection using Beam Loss Monitors

The strategy for machine protection at LHC is based on the measurement of beam loss with dedicated Beam Loss Monitors (BLMs). When a high energy particle is lost, it will produce a particle shower whose energy is partially absorbed in the surrounding magnet coil but part of which can be detected by the BLMs. As long as the calibration factor of energy deposition in the magnet coils with respect to the energy deposited in the BLM is known, the BLM signals can be used to trigger beam dumps as soon as the energy deposition in the magnets gets to a level where a magnet quench must be feared. By dumping the beam and thus avoiding a quench, long beam downtime can be avoided. For even bigger beam losses, where the magnets or other equipment are at risk of destruction, this is even more true.

[1] Rüdiger Schmidt, http://rudi.home.cern.ch/rudi/docs/VisitLHCWuppertal2006.ppt

On the other hand the levels for triggering beam dumps must not be set too low because this may prevent running the machine altogether.

In order to set the trigger levels correctly the allowable losses must be known. These depend on the energy of the primary particle and on the loss duration as can be seen from Figure 9-3. It is therefore important to integrate the measured losses over several time periods and set corresponding thresholds for each of these integration periods. Only like this short and strong losses can be treated as well as smaller but prolonged losses.

For safety systems, in addition to the standard technical specifications like dynamic range, resolution, response time etc, the *Mean Time Between Failur*e (MBTF) is an important parameter. It defines how secure the system actually is. When the security system fails itself it must go into a failsafe state, which, as a consequence, makes the protected system unavailable.

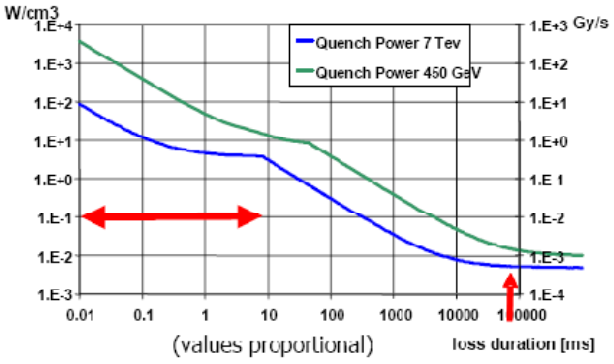

Figure 9-3: Quench levels

Most of today's machine protection systems use ionisation chambers as their BLMs (the LHC BLM can be seen in Figure 9-2). These are gas filled detectors (N_2 in case of the LHC BLMs) with the following properties:

- High dynamic range (10^8)
- Very good resistance to radiation (several MGray/year)
- High reliability and availability

The BLM signal is integrated using a charge balanced integrator and converted to a proportional frequency with a current to frequency converter (CFC). This method allows handling of a very high dynamic range. The CFC frequency is counted over a period of 40 µs. For very low currents and to allow faster response an ADC was added. The converted signal is transported from the machine, some 80m underground to the surface through optical fibres. 8 detectors are multiplexed onto an optical link and the links are doubled. The digital signal treatment is performed by a radiation resistant FPGA which:

- Reads out the converted signal
- Encodes the values in order to prepare them for transmission over the redundant optical serial links
- Multiplexes values from 8 detectors onto a signal transmission channel
- Performs CRC calculations

The electronics on the surface receives the values from the optical links, checks the CRC, de-multiplexes the signals from the 8 BLMs and gives access to the beam loss values through the VME bus. It also connects to the Beam Interlock System (BIC) generating beam dumps, should this be necessary.

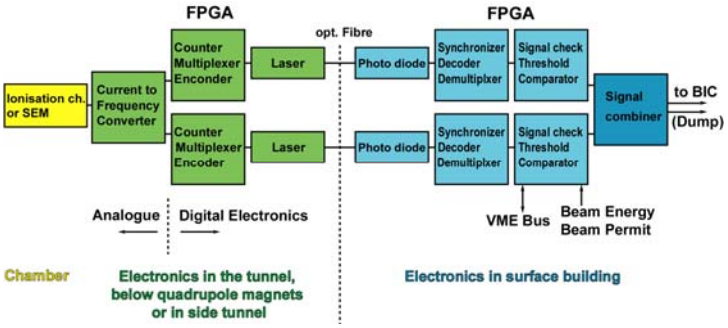

Figure 9-4: Layout of the BLM electronics

9.2 The Data Acquisition Board

Already several times during this lecture we have seen an electronics layout consisting of ADCs, an FPGA reading out the converted signals and treating them through fast digital signal processing algorithms implemented as VHDL code in the FPGA, followed by memory, used to store the final result. Some sort of access to this memory is needed in order to further treat the result and make it available on the operator consoles in the control room in form of easily readable numerical values, tables or graphs.

The requirement of FPGAs connected to some sort of external signal in conjunction with access to the final stored data is general enough to allow the design of a generic card which can be used for a variety of applications.

Figure 9-6: Photo of the Data Acquisition Board

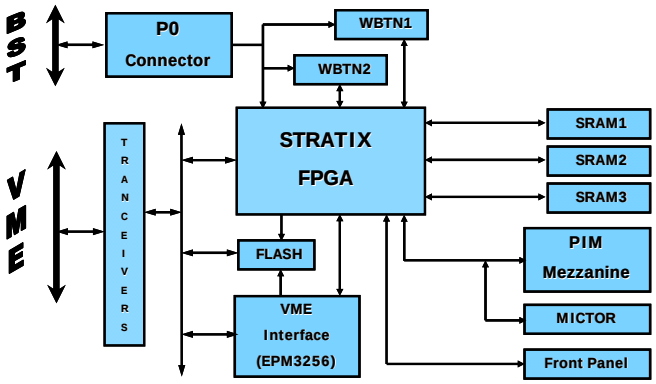

Figure 9-7: Block diagram of the Data Acquisition Board

The Data Acquisition Board (DAB) is implemented as a VME board built around an Altera Stratix FPGA. The FPGA can be boot-strapped through a flash memory containing the FPGA code. This memory is also accessible via the VME bus. In addition external timing signals (Beam Synchronous Timing (BST)) can be accessed by the FPGA and used within the FPGA algorithms. In order to be as flexible as possible the FPGA has access to a local mezzanine bus. Mezzanine boards implement the application specific hardware. Like this the DAB can be used to treat signals from the orbit system, based on several thousands of BPMS, it can be used by intensity measurements systems where signals from beam current transformers are treated or it can be used to handle the communication protocol in order to read out signals from the beam loss system.

9.3 **Data treatment for the Beam Loss System**

9.3.1 Data treatment in the tunnel

The signal coming from the BLM is converted into frequency for coarse conversion, where a counter is used to get the final coarse value. The voltage measured on the ADC is the remainder between the last count and the first count from the next acquisition. Before sending these data to the optical communication channels, the ADC and counter data are combined to a 20 bit loss figure. Eight such values are encoded, multiplexed and sent to the surface electronics after a CRC value has been added.

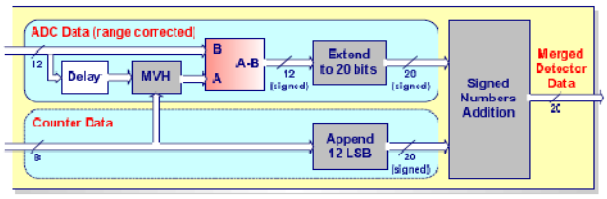

Figure 9-8: Beamloss dynamic range

9.3.2 Data treatment on the surface

The data treatment algorithms in the DAB, installed at the surface must perform the following actions:

- Receive the values from the electronics in the tunnel via the optical fibers
- De-multiplex the data coming from different BLMs
- Check the CRC and compare the data coming from the redundant communication channels. If the data from the two channels differ: decide which one is right
- Calculate successive sums in order to see fast big losses as well as slow small losses.
- Compare the successive sums to threshold values in order to trigger beam dumps should the losses be too high
- Give access to beam loss data for inspection in the control room together with status information
- Keep measured data in a circular buffer for post mortem analysis
- Provide error reporting

As can be seen from Figure 9-3 the threshold levels above which a beam dump must be triggered, depend on the beam energy and the loss duration. For this reason the loss values are integrated using running sums. 12 integration periods, spanning from 40 µs to 84 s are made available.

The calculation of running sums is rather simple. Each incoming value is added to a register, while the oldest value of the interval is subtracted again. Of course all values making up the sum must be kept.

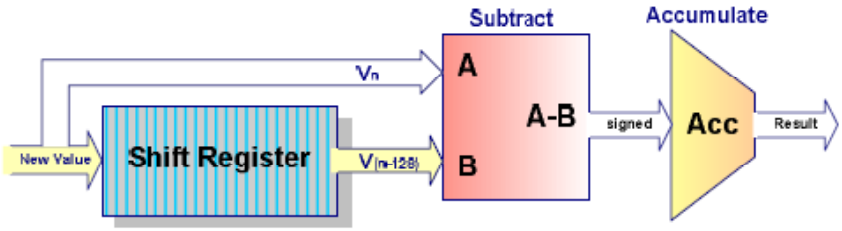

Figure 9-9: Calculating running sums

Another way to handle the calculations would be to use a long shift register and always add the difference between the first and the last values.

The longer the integration interval, the longer the shift register must become. This problem can be overcome by using partial sums instead of keeping all previous values. This results in a cascade of shift registers and adders as shown in Figure 9-10. In addition a multi-point shift register is used calculating 2 running sums at once.

Of course the latency of the sum output for each running sum depends on the time the previous sum needs for its calculation and increases therefore for longer integration periods. The running sums are compared to threshold values, dependent on the particle energy and a dump trigger is issued if the losses exceed those threshold values.

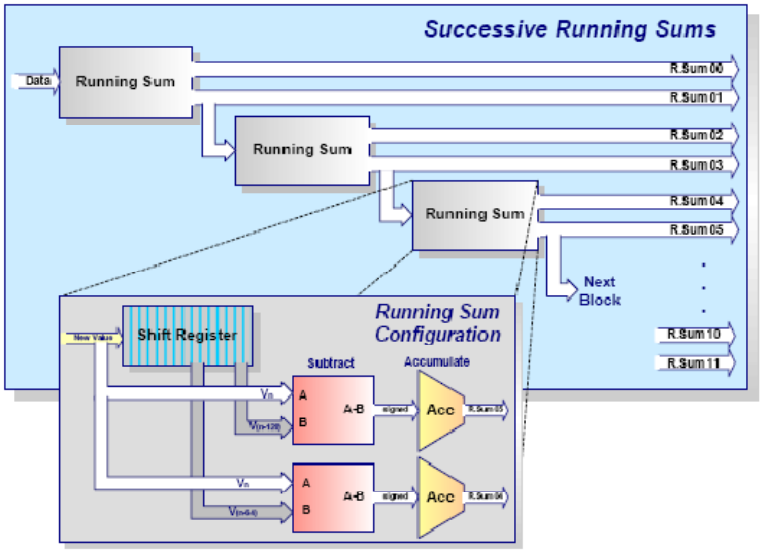

Figure 9-10: Cascade of running sums

Apart from triggering beam dumps the loss values are used for online viewing and logging as well as for post-mortem analysis. The values for the last 20000 turns (40 μs samples) as well as the 82 ms summed values of acquired data during the last 45 mins are available. In addition status information about the functioning of each individual BLM station is transferred from the tunnel to the surface electronics allowing online supervision of the whole system.

Part of the recorded data will be used

- to drive an on-line event display in the control room and
- write an extensive logging database both at a refresh rate of 1Hz.

Other parts of the same processing units, initiated by external triggers, will provide fast updates of the loss pattern seen. For example:

- For the automated collimator adjustments, it will record and provide the last 20ms by 640us integrals.
- At every beam injection and scheduled dump, 100ms worth of data will be pushed to the relevant systems to be used to verify the correctness of those procedures, and
- A detailed post-mortem analysis study will be possible, in the event of an unforeseen dump, by analyzing the last 1.7s by 40us integrals stored in the electronics for each channel.

10. FURTHER READING

The Joint Universities Accelerator School (JUAS) is an accelerator physics course which is held every year for 4 weeks in Archamps, France. It extends the university physics curriculum with an academic course, that would be difficult to organise at European Universities and is open to students from all European countries. It teaches all fields of machine physics and accelerator technologies, and beam diagnostics is one of the topics. P. Forck from Gesellschaft für Schwerionenforschung (GSI) Darmstadt, Germany, has taught this subject for several years and he has written excellent course notes, which are available at http://www-bd.gsi.de/conf/juas/juas.html together with the course transparencies.

Earlier CAS courses contain articles on beam diagnostics, namely the one of Jyväskylä with a chapter on beam instrumentation written by H. Koziol.

In 1998 and 2008 there were CAS schools dedicated to Beam Measurement and their proceedings provide more elaborate explanations on how machine parameters may be measured.

For detailed descriptions of measurement techniques or instruments, the proceedings of the bi-annual beam diagnostics conferences DIPAC (Diagnostics and Instrumentation for Particle Accelerators in Europe) and BIW (Beam Instrumentation Workshop in the USA) are interesting sources of information.

CONCLUSION

In two hours of lectures it is only possible to give a crude overview of the field of beam diagnostics. There is a multitude of different measuring principles and instruments and I tried to touch at least on a few of them, emphasizing peculiarities of low energy machines, like big beam sizes, long pulses etc. I hope that these lectures convinced you that beam diagnostics is a fascinating field of accelerator technology and that they made you curious to further explore this scientific field.

ACKNOWLEDGEMENTS

I would like to thank E. Bravin, T. Lefevre, and V. Prieto, J. Belleman, M. Gasior, L. Søby, P. Odier, C. Bal, P. Forck for interesting discussions, help by providing their tables, figures or photographs or proof reading. Further thanks go to my group leader R. Jones, who allowed me to put the necessary effort into the preparation of these lectures and to my wife who saw me typing away on my computer for many long evenings.

TABLE OF CONTENTS

LIST OF FIGURES